Journal of Molecular Structure 1214 (2020) 128149

Contents lists available at ScienceDirect

Journal of Molecular Structure

journal homepage: http://www.elsevier.com/locate/molstruc

New allyldithiocarbimate salts: Synthesis, structure and antifungal activity

Nathália M. Albuini-Oliveira [a], Mayura M.M. Rubinger [a, *], Silvana Guilardi [b], Rafael A.C. Souza [b], Javier Ellena [c], Natalia Alvarez [d], Eder C. Tavares [e], Carlos H.C. Zacchi [f], Antonio E.C. Vidigal [a], Marcelo S. Lima [a], Laercio Zambolim [g]

[a] Departamento de Química, Universidade Federal de Viçosa, 36570-900 Viçosa, MG, Brazil
[b] Instituto de Química, Universidade Federal de Uberlândia, 39400-902 Uberlândia, MG, Brazil
[c] Instituto de Física de São Carlos, Universidade de São Paulo, 13566-590 São Carlos, SP, Brazil
[d] Facultad de Química, Universidad de la República, General Flores 2124, Montevideo, Uruguay
[e] Instituto de Física e Química, Universidade Federal de Itajubá, 37500-903 Itajubá, MG, Brazil
[f] Departamento de Química, Centro Federal de Educação Tecnológica de Minas Gerais, 30421-169 Belo Horizonte, MG, Brazil
[g] Departamento de Fitopatologia, Universidade Federal Viçosa, 36570-900 Viçosa, MG, Brazil

ARTICLE INFO

Article history:
Received 6 December 2019
Received in revised form
25 February 2020
Accepted 27 March 2020
Available online 6 April 2020

Keywords:
Allyldithiocarbimates
Crystal structure
Hirshfeld surface
Antifungal activity

ABSTRACT

Fifteen new allyldithiocarbimates were prepared from different allylic bromides and various potassium dithiocarbimates, yielding (*Z*)-2-(methoxycarbonyl)-3-(X-nitrophenyl)allyl-(*N*-R-sulfonyl)dithiocarbimates (where X = 2, 3 and 4; R = phenyl, 4-fluorophenyl, 4-chlorophenyl, 4-bromophenyl and 4-iodophenyl). These anions were isolated as tetraphenylphosphonium salts and characterized by HRMS, infrared, ^{1}H and ^{13}C NMR spectroscopies. Molecular electrostatic potentials were used to evaluate intermolecular interactions present in the new substances and to explain variations observed on their melting points. Single crystal X-ray diffraction experiments confirmed the *Z* stereochemistry of the allyldithiocarbimate anions. C–H···O, C–H···N, C–H···S and C–H···π intermolecular interactions in the solid state were studied by X-ray diffraction and Hirshfeld surface analyses. The new compounds inhibited the mycelial growth of various fungi species responsible for severe plant diseases. The allylithiocarbimates were especially active against *Botrytis cinerea*, with IC_{50} values as low as 20 μM, being more effective than the active principals of the commercial fungicides Ziram and Mancozeb.

1. Introduction

Phytopathogenic fungi that cause significant losses pose one of the biggest challenges in the agricultural sector. The most efficient methods to control diseases in crops include the use of agrochemicals. Among such compounds, the dithiocarbamates ($R_2NCS_2^{1-}$) are protective broad-spectrum fungicides, with relatively low toxicity to non-target organisms [1,2]. There are few reports of resistance to fungicides with multiple sites of action. For example, zinc and manganese dithiocarbamates such as Ziram and Mancozeb have been in the market for decades [2–4]. Dithiocarbamates also have industrial applications, mainly as accelerators of the vulcanization of natural rubber [5].

Although chemically similar to the dithiocarbamates, the dithiocarbimates ($RN{=}CS_2^{2-}$) do not have commercial applications yet. We have recently described that dithiocarbimates can act as nucleophiles in organic reactions producing allyldithiocarbimates [6]. The expressive activity against *Botrytis cinerea* of the salt shown in Fig. 1 [6] indicated that further studies on the allyldithiocarbimates could lead to new metal-free protectant agrochemicals, as *B. cinerea* is one of the top ten most scientifically and economically important fungi, with devastating effects on crops [7].

Thus, we became very interested in understanding the chemistry and the structural properties of this new class of potential agrochemicals. This work describes the syntheses and structural studies of fifteen allyldithiocarbimate salts. These new compounds were fully characterized by elemental analysis, HRMS, infrared, ^{1}H and ^{13}C NMR spectroscopies. Single crystal X-ray diffraction, molecular electrostatic potentials and Hirshfeld surface analyses allowed a better insight into their intermolecular interactions in the

* Corresponding author.
E-mail address: mayura@ufv.br (M.M.M. Rubinger).

https://doi.org/10.1016/j.molstruc.2020.128149
0022-2860/

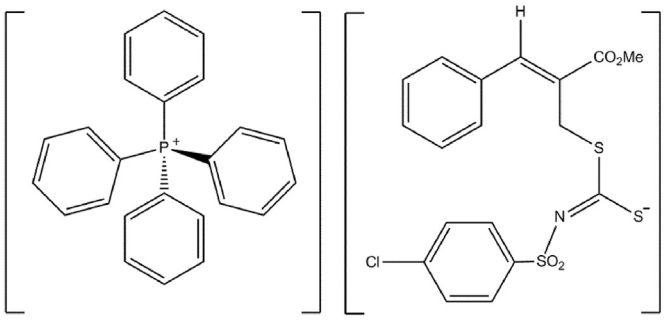

Fig. 1. A biologically active allyldithiocarbimate salt [6].

solid state and confirmed the stereochemistry of the allyldithiocarbimates indicated by the spectroscopic data. We have also deepened the studies on the biological activity of the allyldithiocarbimates against phytopatogenic fungi.

2. Experimental

2.1. Methods and materials

Melting points were determined with MQAPF-302 Microquimica apparatus, without correction. IR spectra were recorded on a Varian 660 FT-IR (ATR) spectrometer. ^{1}H NMR (300 MHz), ^{13}C (75 MHz) data were obtained with a VARIAN MERCURY 300 spectrometer, from solutions in deuterated chloroform ($CDCl_3$) or dimethyl sulfoxide (DMSO-d_6), with tetramethylsilane (TMS) as internal reference. Exact mass was determined by high-resolution electrospray ionization mass spectrometry (HR-ESI-MS) in acetonitrile solutions by direct infusion method using a Bruker Daltonics MicroTOF-QII-ESI-QQ-TOF mass spectrometer. Microanalyses for C, H and N were obtained from a Leco TruSpec Micro CHN elemental analyzer.

The key intermediates were prepared as shown in Scheme 1. The benzenesulfonamide, 4-chlorobenzenesulfonamide, 4-bromobenzenesulfonamide were purchased from Sigma-Aldrich. The 4-fluorobenzenesulfonamide and 4-iodobenzenesulfonamide were prepared from the respective sulfonyl chlorides in reaction with concentrated ammonia solution, as described in the literature [8]. Then, potassium dithiocarbimates, $K_2(RSO_2N{=}CS_2)$, where R = C_6H_5, 4-FC_6H_4, 4-ClC_6H_4, 4-BrC_6H_4 and 4-IC_6H_4 were prepared by reacting the appropriate sulfonamides with carbon disulfide and potassium hydroxide (Scheme 1) as described in the literature [9–14]. Morita-Baylis-Hillman (MBH) adducts were prepared from the reaction of 4-nitrobenzaldehyde, 3-nitrobenzaldehyde or 2-nitrobenzaldehyde with methyl acrylate, catalyzed by 1,4-diazabicyclo[2.2.2]octane (DABCO) [15]. The MBH adducts, in reaction with lithium bromide and sulfuric acid in acetonitrile, yielded the respective allylic bromides (Scheme 1) [16–18]. All reactions were monitored by thin-layer chromatography (TLC) with Macherey-Nagel silica gel (0.25 mm) plates pre-coated on Polygram polyester sheets, with fluorescent indicator (254 nm). The MBH adducts and the allylic bromides were purified by column chromatography on silica gel 60 (70–230 mesh), using hexane and ethyl acetate as eluents. The infrared spectra and melting points of the allylic bromides and the potassium dithiocarbimates were in accordance with the literature [9–14,16–18].

2.2. Synthesis of the allyldithiocarbimate salts

The syntheses of the new compounds were performed as shown in Scheme 2.

A solution of the appropriated allylic bromide (1 mmol) in acetone (2 mL) was added dropwise to stirring solutions of the potassium *N*-R-sulfonyldithiocarbimates (1.2 mmol) in acetone:-water 1:1 (10 mL). The mixture (monitored by TLC) was stirred for *ca.* 15 min at room temperature. Then, water (5 mL) was added and extractions with ethyl acetate (3 × 20 mL) were performed. The combined organic extracts were concentrated under reduced pressure and the residue was dissolved in water (20 mL). Tetraphenylphosphonium chloride (1 mmol) was added to this aqueous solution and the mixture was stirred for *ca.* 10 min. The yellow solids thus formed (compounds **1A**-**E**, **2A**-**E**, **3A**-**E**) were filtered out of the mixtures, washed with distilled water and dried under reduced pressure for one day.

2.2.1. Tetraphenylphosphonium (Z)-2-(methoxycarbonyl)-3-(4-nitrophenyl)allyl-(N-phenylsulfonyl)dithiocarbimate (**1A**)

Yield = 92%; mp = 156.9–158.1 °C; IR (ATR, cm^{-1}) $\bar{\upsilon}_{max}$ 3066, 3018, 2956, 1725, 1625, 1591, 1522, 1490, 1440, 1383, 1340, 1271, 1261, 1230, 1203, 1133, 1110, 1085, 1068, 995, 975, 933, 844, 784, 755, 723, 686, 636, 565, 523; ^{1}H NMR (300 MHz, $CDCl_3$): δ 3.76 (s, 3H, OCH_3), 4.20 (s, 2H, H1), 7.33–7.34 (m, 3H, H2′, H4′, H6′), 7.58–7.72 (m, 11H, H3′, H5′, H3, Hb, Hf), 7.73–7.85 (m, 10H, H5, H9, Hc, He), 7.87–7.98 (m, 4H, Hd), 8.10 (d, 2H, $^{3}J_{6,5} = {}^{3}J_{8,9}$ = 9 Hz, H6, H8); ^{13}C NMR (75 MHz, $CDCl_3$): δ 33.4 (C1), 52.7 (OCH_3), 117.7 (d, $^{1}J_{Ca\text{-}P}$ = 89 Hz, Ca), 123.9 (C6, C8), 127.8 (C2′, C6′), 128.2 (C3′, C5′), 130.7 (C4′), 131.0 (d, $^{2}J_{Cb,Cf\text{-}P}$ = 12.8 Hz, Cb, Cf), 131.1 (C2), 131.9 (C5, C9), 134.6 (d, $^{3}J_{Ce,Cc\text{-}P}$ = 9.8 Hz, Cc, Ce), 136.0 (d, $^{4}JC_{d\text{-}P}$ = 3 Hz, Cd), 138.0 (C3), 141.7 (C4), 143.7 (C1'), 147.5 (C7), 167.8 (C=O), 200.7 (C=N); HR-ESI-MS, *m/z*: Calcd for $C_{18}H_{15}N_2O_6S_3^{2-}$: 451.0092, found 451.0105. Elemental analysis: Found (calculated for $C_{42}H_{35}N_2O_6PS_3$): C, 63.30 (63.78); H, 4.53 (4.46) and N, 3.69 (3.54)

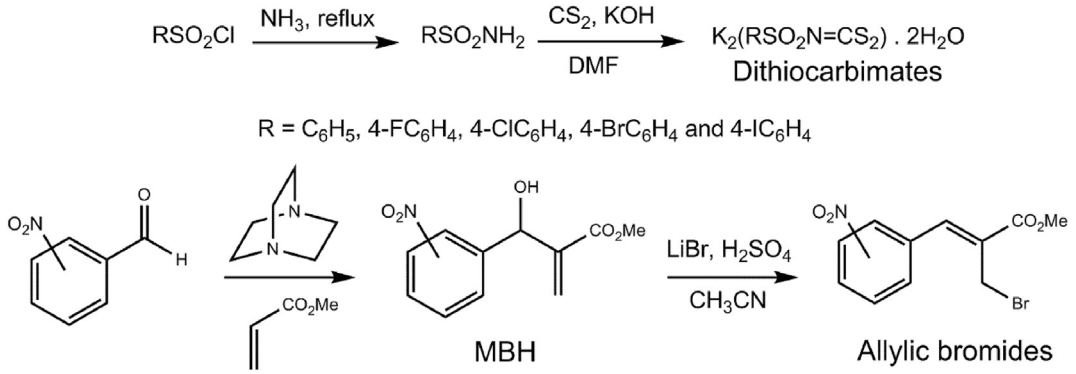

Scheme 1. Preparation of the synthetic intermediates.

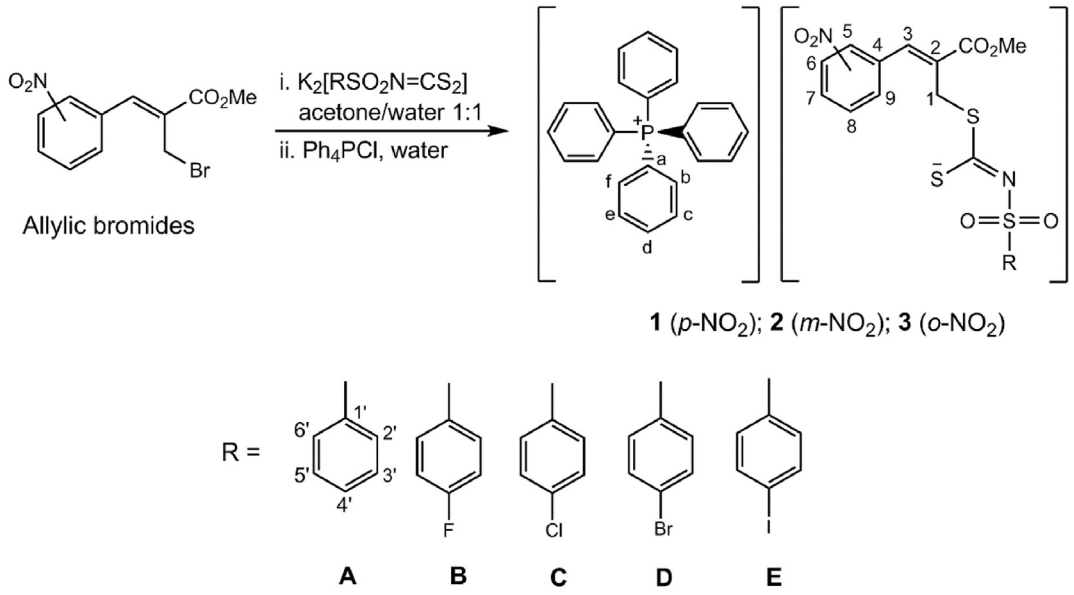

Scheme 2. Syntheses of tetraphenylphosphonium allyldithiocarbimates and the numbering used for the NMR attributions.

%.

*2.2.2. Tetraphenylphosphonium (Z)-2-(methoxycarbonyl)-3-(4-nitrophenyl)allyl-(N-4-fluorophenylsulfonyl)dithiocarbimate (**1B**)*

Yield = 95%; mp = 147.7–148.9 °C; IR (ATR, cm^{-1}) $\bar{\upsilon}_{max}$ 3060, 3021, 2956, 1723, 1625, 1591, 1522, 1490, 1438, 1383, 1344, 1271, 1261, 1227, 1203, 1133, 1110, 1085, 1068, 995, 975, 935, 844, 781, 751, 725, 686, 636, 563, 526; ^{1}H NMR (300 MHz, $CDCl_3$): δ 3.76 (s, 3H, OCH_3), 4.19 (s, 2H, H1), 6.95 (t, 2H, $^3J_{3',2'} = {}^3J_{5',6'} = {}^3J_{3',5',F} = 9$ Hz, H3′, H5′), 7.56–7.73 (m, 9H, H3, Hb, Hf) 7.75–7.86 (m, 10H, Hc, He, H5, H9), 7.88–7.99 (m, 6H, H2′, H6′, Hd), 8.11 (d, 2H, $^3J_{6,5} = {}^3J_{8,9} = 6$ Hz, H6, H8); ^{13}C NMR (75 MHz, $CDCl_3$): δ 33.4 (C1), 52.8 (OCH_3), 114.6 (d, $^2J_{C3',C5'-F} = 22.5$ Hz, C5′, C3′), 117.7 (d, $^1J_{Ca-P} = 90$ Hz, Ca), 123.9 (C6, C8), 130.8 (d, $^3J_{F-C2',C6'} = 9.0$ Hz, C2′, C6′), 131.0 (d, $^2J_{Cb,Cf-P} = 12.8$ Hz, Cb, Cf, C5, C9), 131.8 (C2), 134.6 (d, $^3J_{Ce,Cc-P} = 9.8$ Hz, Cc, Ce), 136.0 (d, $^4J_{Cd-P} = 3$ Hz, Cd), 138.0 (C3), 139.6 (d, $^4J_{C1'-F} = 2.3$ Hz, C1′), 141.6 (C4), 147.5 (C7), 164.1 (d, $^1J_{C4'-F} = 252.8$ Hz, C4′), 167.8 (C=O), 201.5 (C=N); HR-ESI-MS, *m/z*: Calcd for $C_{18}H_{14}FN_2O_6S_3^{2-}$: 469.0004, found 469.0010. Elemental analysis: Found (calculated for $C_{42}H_{34}FN_2O_6PS_3$): C, 62.72 (62.36); H, 4.31 (4.24) and N, 3.33 (3.46) %.

*2.2.3. Tetraphenylphosphonium (Z)-2-(methoxycarbonyl)-3-(4-nitrophenyl)allyl-(N-4-chlorophenylsulfonyl)dithiocarbimate (**1C**)*

Yield = 90%; mp = 140.0–141.2 °C; IR (ATR, cm^{-1}) $\bar{\upsilon}_{max}$ 3055, 2955, 1707, 1589, 1515, 1481, 1436, 1357, 1344, 1256, 1137, 1109, 1085, 1067, 997, 934, 852, 831, 778, 751, 725, 686, 662, 619, 565, 526, 479; ^{1}H NMR (300 MHz, $CDCl_3$): δ 3.76 (s, 3H, OCH_3), 4.20 (s, 2H, H1), 7.25 (d, 2H, $^3J_{3',2'} = {}^3J_{5',6'} = 9$ Hz, H2′, H6′), 7.56–7.73 (m, 9H, H3, Hb, Hf) 7.75–7.86 (m, 10H, Hc, He, H5, H9), 7.88–7.91 (m, 6H, H3′, H5′, Hd), 8.11 (d, 2H, $^3J_{6,5} = {}^3J_{8,9} = 6$ Hz, H6, H8); ^{13}C NMR (75 MHz, $CDCl_3$): δ 33.5 (C1), 52.7 (OCH_3), 117.7 (d, $^1J_{Ca-P} = 85.5$ Hz, Ca), 123.9 (C6, C8), 127.8 (C2′, C6′), 129.9 (C3′, C5′), 131.0 (d, $^2J_{Cb,Cf-P} = 12.8$ Hz, Cb, Cf, C5, C9), 131.7 (C2), 134.6 (d, $^3J_{Ce,Cc} = 9.8$ Hz, Cc, Ce), 136.0 (d, $^4J_{Cd-P} = 3$ Hz, Cd), 136.1 (C4′), 138.1 (C3), 141.7 (C4), 142.1 (C1'), 147.5 (C7), 167.8 (C=O), 201.5 (C=N); HR-ESI-MS, *m/z*: Calcd for $C_{18}H_{14}ClN_2O_6S_3^{2-}$: 484.9708, found 484.9712. Elemental analysis: Found (calculated for $C_{42}H_{34}ClN_2O_6PS_3$): C, 59.55 (61.12); H, 4.12 (4.15) and N, 3.40 (3.39) %.

*2.2.4. Tetraphenylphosphonium (Z)-2-(methoxycarbonyl)-3-(4-nitrophenyl)allyl-(N-4-bromophenylsulfonyl)dithiocarbimate (**1D**)*

Yield = 88%; mp = 105.5–107.0 °C; IR (ATR, cm^{-1}) $\bar{\upsilon}_{max}$ 3055, 2953, 1708, 1591, 1575, 1514, 1483, 1436, 1357, 1344, 1257, 1137, 1110, 1081, 1068, 1010, 997, 939, 848, 824, 778, 755, 721, 686, 604, 558, 520, 414; ^{1}H NMR (300 MHz, $CDCl_3$): δ 3.78 (s, 3H, OCH_3), 4.21 (s, 2H, H1), 7.43 (d, 2H, $^3J_{3',2'} = {}^3J_{5',6'} = 9$ Hz, H2′, H6′), 7.58–7.73 (m, 9H, H3, Hb, Hf) 7.73–7.84 (m, 10H, Hc, He, H5, H9), 7.87–7.92 (m, 6H, H3′, H5′, Hd), 8.14 (d, 2H, $^3J_{6,5} = {}^3J_{8,9} = 6$ Hz, H6, H8); ^{13}C NMR (75 MHz, $CDCl_3$): δ 33.5 (C1), 52.6 (OCH_3), 117.6 (d, $^1J_{Ca-P} = 89.3$ Hz, Ca), 123.9 (C6, C8), 125.3 (C4′), 130.1 (C2′, C6′), 130.9 (C3′, C5′), 131.0 (d, $^2J_{Cb,Cf-P} = 12.8$ Hz, Cb, Cf, C5, C9), 131.7 (C2), 134.6 (d, $^3J_{Ce,Cc-P} = 10.5$ Hz, Cc, Ce), 136.0 (d, $^4J_{Cd-P} = 3$ Hz, Cd), 138.2 (C3), 141.6 (C4), 142.6 (C1'), 147.5 (C7), 167.8 (C=O), 201.6 (C=N); HR-ESI-MS, *m/z*: Calcd for $C_{18}H_{14}BrN_2O_6S_3^{2-}$: 530.9177, found 530.9190. Elemental analysis: Found (calculated for $C_{42}H_{34}BrN_2O_6PS_3$): C, 56.40 (58.00); H, 4.06 (3.94) and N, 3.56 (3.22) %.

*2.2.5. Tetraphenylphosphonium (Z)-2-(methoxycarbonyl)-3-(4-nitrophenyl)allyl-(N-4-iodophenylsulfonyl)dithiocarbimate (**1E**)*

Yield = 95%; mp = 130.0–131.8 °C; IR (ATR, cm^{-1}) $\bar{\upsilon}_{max}$ 3055, 2950, 1708, 1594, 1567, 1514, 1484, 1435, 1344, 1260, 1203, 1140, 1106, 1079, 940, 852, 810, 755, 725, 685, 600, 559, 526; ^{1}H NMR (300 MHz, $CDCl_3$): δ 3.78 (s, 3H, OCH_3), 4.21 (s, 2H, H1), 7.43 (d, 2H, $^3J_{3',2'} = {}^3J_{5',6'} = 9$ Hz, H2′, H6′), 7.59–7.71 (m, 11H, H3, H3′, H5′, Hb, Hf) 7.73–7.81 (m, 10H, Hc, He, H5, H9), 7.87–7.92 (m, 4H, Hd), 8.14 (d, 2H, $^3J_{6,5} = {}^3J_{8,9} = 9$ Hz, H6, H8); ^{13}C NMR (75 MHz, $CDCl_3$): δ 33.5 (C1), 52.9 (OCH3), 97.7 (C4′), 117.7 (d, $^1J_{Ca-P} = 88.5$ Hz, Ca), 123.9 (C6, C8), 130.1 (C2′, C6′), 131.0 (d, $^2J_{Cb,Cf-P} = 12.8$ Hz, Cb, Cf, C5, C9), 131.7 (C2), 134.6 (d, $^3J_{Ce,Cc-P} = 10.5$ Hz, Cc, Ce), 136.0 (d, $^4J_{Cd-P} = 3$ Hz, Cd), 136.9 (C3′, C5′), 138.2 (C3), 141.6 (C4), 143.3 (C1'), 147.5 (C7), 167.9 (C=O), 201.5 (C=N); HR-ESI-MS, *m/z*: Calcd for $C_{18}H_{14}IN_2O_6S_3^{2-}$: 576.9064, found 576.9087. Elemental analysis: Found (calculated for $C_{42}H_{34}IN_2O_6PS_3$): C, 54.73 (55.02); H, 3.77 (3.74) and N, 3.20 (3.06) %.

*2.2.6. Tetraphenylphosphonium (Z)-2-(methoxycarbonyl)-3-(3-nitrophenyl)allyl-(N-phenylsulfonyl)dithiocarbimate (**2A**)*

Yield = 97%; mp = 136.4–137.0 °C; IR (ATR, cm^{-1}) $\bar{\upsilon}_{máx}$ 3066, 2950, 1705, 1529, 1433, 1371, 1353, 1275, 1209, 1141, 1110, 1085, 947,

Table 1
Crystallographic data and details of diffraction experiments for compounds **1A**, **2A** and **3A**.

Compound	**1A**	**2A**	**3A**
Empirical formula	$C_{42}H_{35}N_2O_6PS_3$	$C_{42}H_{35}N_2O_6PS_3$	$C_{42}H_{35}N_2O_6PS_3$
Formula weight (g mol l^{-1})	790.87	790.87	790.87
Temperature (K)	296(2)	296(2)	296(2)
Crystal system	Monoclinic	Triclinic	Monoclinic
Space group	$P2_1$	$P\bar{1}$	P2/c
Unit cell dimensions			
a (Å)	7.7510(3)	10.1543(8)	22.0350(7)
b (Å)	37.121(1)	12.896(1)	7.4667(2)
c (Å)	26.9375(8)	14.696(1)	25.0990(7)
α (°)	90	93.251(6)	90
β (°)	90.131(2)	94.626(7)	111.032(2)
γ (°)	90	104.879(6)	90
Volume ($Å^3$), Z	7750.5(4), 2	1848.0(3), 2	3854.4(2), 4
Calculated density (g cm^{-3})	1.359	1.421	1.363
μ (mm^{-1})	2.556	0.297	0.285
T_{min}/T_{max}	0.629/0.784	0.6695/0.7456	0.916/0.969
F(000)	3312	824	1648
Crystal size (mm)	0.200 × 0.120 × 0.100	0.197 × 0.135 × 0.023	0.315 × 0.218 × 0.110
θ range (°)	2.891 to 75.053	3.121 to 30.507	0.990 to 27.498
Limiting indices	−9,9; 0,46; −33,33	−14,14; −14,18; −20,20	−28,28; −9,9; −32,32
Reflections collected	30978	22845	34003
Independent reflections	16078 [R(int) = 0.0757]	11203 [R(int) = 0.0548]	8845 [R(int) = 0.0428]
Goodness	1.088	1.058	1.017
Data/restraints/parameters	10782/490/1935	7286/0/487	5999/0/488
R indices [$I > 2\sigma(I)$]	R = 0.0790, w*R* = 0.1445	R = 0.0629, w*R* = 0.1445	R = 0.0513, w*R* = 0.1173
R indices (all data)	R = 0.1169, w*R* = 0.1614	R = 0.1116, w*R* = 0.1724	R = 0.0832, w*R* = 0.1353
Largest diff. peak and hole (e A^{-3})	0.440 and −0.326	0.541 and −0.546	0.316 and −0.255

$R = \Sigma\,(||F_o| - |F_c||)/\Sigma|F_o|$; $wR = [\Sigma w(|F_o^2| - |F_c^2|)^2/\Sigma w|F_o^2|^2]^{1/2}$.

931, 825, 14, 721, 689, 675, 580, 558, 526; ^{1}H NMR (300 MHz, DMSO-d_6): δ 3.77 (s, 3H, OCH_3), 4.07 (s, 2H, H1), 7.39–7.44 (m, 3H, H2′, H4′, H6′), 7.72–8.06 (m, 25H, Hb, Hc, Hd, He, Hf, H3, H7, H8, H3′, H5′), 8.19–8.29 (m, 1H, H9), 8.37 (s, 1H, H5); ^{13}C NMR (75 MHz, DMSO): δ 32.2 (C1), 52.2 (OCH_3), 117.6 (d, $^1J_{Ca\text{-}P}$ = 88.5 Hz, Ca), 123.4 (C7), 124.3 (C5), 127.2 (C2′, C6′), 127.5 (C3′, C5′), 130.1 (C2, C8), 130.3 (d, $^2J_{Cb,Cf\text{-}P}$ = 12.8 Hz, Cb, Cf), 130.4 (C4′), 134.4 (d, $^3J_{Cc,Ce\text{-}P}$ = 10.5 Hz, Cc, Ce), 135.2 (d, $^4J_{Cd\text{-}P}$ = 3 Hz, Cd), 135.5 (C9), 135.9 (C4), 137.3 (C3), 143.4 (C1'), 147.8 (C6), 166.8 (C=O), 198.1 (C=N); HR-ESI-MS, *m/z*: Calcd for $C_{18}H_{15}N_2O_6S_3^{2-}$: 451.0092, found 451.0020. Elemental analysis: Found (calculated for $C_{42}H_{35}N_2O_6PS_3$): C, 63.81 (63.78); H, 4.49 (4.46) and N, 3.51 (3.54) %.

2.2.7. Tetraphenylphosphonium (Z)-2-(methoxycarbonyl)-3-(3-nitrophenyl)allyl-(N-4-fluorophenylsulfonyl)dithiocarbimate (**2B**)

Yield = 80%; mp = 131.2–132.8 °C; IR (ATR, cm^{-1}) $\bar{\upsilon}_{max}$ 3079, 3056, 2991, 2933, 1711, 1633, 1589, 1525, 1494, 1481, 1436, 1360, 1351, 1292, 1272, 1225, 1202, 1163, 1141, 1107, 1085, 995, 944, 835, 814, 782, 756, 721, 685, 649, 555, 542, 521; ^{1}H NMR (300 MHz, $CDCl_3$): δ 3.77 (s, 3H, OCH_3), 4.21 (s, 2H, H1), 6.94 (t, 2H, $^3J_{3',2'} = {}^3J_{5',6'} = {}^3J_{3',5',F}$ = 9 Hz, H3′, H5′), 7.57–7.65 (m, 10H, Hb, Hf, H3, H8), 7.73–7.79 (m, 8H, Hc, He), 7.87–7.98 (m, 6H, Hd, H2′, H6′), 8.10 (*pseudo*-t, 2H, H7, H9), 8.16 (s, 1H, H5); ^{13}C NMR (75 MHz, $CDCl_3$): δ 33.0 (C1), 52.4 (OCH_3), 114.4 (d, $^2J_{C3',C5'\text{-}F}$ = 21.8 Hz, C3′,C5′), 117.4 (d, $^1J_{Ca\text{-}P}$ = 89 Hz, Ca), 123.1 (C7), 124.7 (C5), 130.2 (C2), 130.5 (d, $^3J_{C2',C6'\text{-}F}$ = 9 Hz, C2′,C6′), 130.8 (d, $^2J_{Cb,Cf\text{-}P}$ = 12.8 Hz, Cb, Cf), 130.9 (C8), 134.3 (d, $^3J_{Cc,Ce\text{-}P}$ = 10.5 Hz, Cc, Ce), 135.8 (d, $^4J_{Cd\text{-}P}$ = 3, Cd), 135.9 (C9), 136.5 (C4), 137.8 (C3), 139.4 (d, $^4J_{C1'\text{-}F}$ = 3 Hz, C1′), 148.0 (C6), 163.8 (d, $^1J_{C4'\text{-}F}$ = 248 Hz, C4′), 167.6 (C=O), 201.2 (C=N); HR-ESI-MS, *m/z*: Calcd for $C_{18}H_{14}FN_2O_6S_3^{2-}$: 469.0004; found 469.0019. Elemental analysis: Found (calculated for $C_{42}H_{34}FN_2O_6PS_3$): C, 60.81 (62.36); H, 4.23 (4.24) and N, 3.53 (3.46) %.

2.2.8. Tetraphenylphosphonium (Z)-2-(methoxycarbonyl)-3-(3-nitrophenyl)allyl-(N-4-chlorophenylsulfonyl)dithiocarbimate (**2C**)

Yield = 82%; mp = 116.4–117.0 °C; IR (ATR, cm^{-1}) $\bar{\upsilon}_{max}$ 3060, 2949, 1712, 1629, 1583, 1525, 1479, 1435, 1351, 1264, 1205, 1141, 1106, 1082, 947, 816, 752, 720, 676, 615, 559, 526, 474; ^{1}H NMR (300 MHz, $CDCl_3$): δ 3.77 (s, 3H, OCH_3), 4.22 (s, 2H, H1), 7.23 (d, 2H, $^3J_{2',3'} = {}^3J_{5',6'}$ = 9 Hz, H2′, H6′), 7.58–7.64 (m, 10H, Hb, Hf, H3, H8), 7.72–7.79 (m, 8H, Hc, He), 7.87–7.92 (m, 6H, Hd, H3′, H5′), 8.08–8.16 (m, 3H, H5, H7,H9); ^{13}C NMR (75 MHz, $CDCl_3$): δ 33.0 (C1), 52.4 (OCH_3), 117.4 (d, $^1J_{Ca\text{-}P}$ = 88.5 Hz, Ca), 123.1 (C7), 124.7 (C5), 127.6 (C2′, C6′), 129.6 (C3′, C5′), 130.2 (C2), 130.8 (d, $^2J_{Cb,Cf\text{-}P}$ = 12.8 Hz, Cb, Cf), 130.9 (C8), 134.4 (d, $^3J_{Cc,Ce\text{-}P}$ = 10.5 Hz, Cc, Ce), 135.8 (d, $^4J_{Cd\text{-}P}$ = 3 Hz, Cd), 135.9 (C9), 136.3 (C4′), 136.5 (C4), 137.7 (C3), 142.1 (C1'), 148.0 (C6), 167.6 (C=O), 201.4 (C=N); HR-ESI-MS, *m/z*: Calcd for $C_{18}H_{14}ClN_2O_6S_3^{2-}$: 484.9708, found 484.9728. Elemental analysis: Found (calculated for $C_{42}H_{34}ClN_2O_6PS_3$): C, 59.63 (61.12); H, 4.21 (4.15) and N, 3.41 (3.39) %.

2.2.9. Tetraphenylphosphonium (Z)-2-(methoxycarbonyl)-3-(3-nitrophenyl)allyl-(N-4-bromophenylsulfonyl)dithiocarbimate (**2D**)

Yield = 86%; mp = 83.6–85.2 °C; IR (ATR, cm^{-1}) $\bar{\upsilon}_{max}$ 3085, 3055, 2950, 2929, 1712, 1629, 1572, 1481, 1436, 1351, 1268, 1207, 1141, 1106, 1081, 995, 948, 816, 781, 720, 685, 601, 559, 522, 412; ^{1}H NMR (300 MHz, $CDCl_3$): δ 3.77 (s, 3H, OCH_3), 4.20 (s, 2H, H1), 7.39 (d, 2H, $^3J_{2',3'} = {}^3J_{5',6'}$ = 9 Hz, H2′, H6′), 7.55–7.65 (m, 10H, Hb, Hf, H3, H8), 7.72–7.82 (m, 10H, Hc, He, H3′, H5′), 7.86–7.91 (m, 4H, Hd), 8.07 (*pseudo*-t, 2H, H7, H9), 8.17 (s, 1H, H5); ^{13}C NMR (75 MHz, $CDCl_3$): δ 32.0 (C1), 52.4 (OCH_3), 117.4 (d, $^1J_{Ca\text{-}P}$ = 89 Hz, Ca), 123.1 (C7), 124.7 (C5), 125.0 (C4′), 129.7 (C2′, C6′), 130.1 (C2), 130.7 (C8, C3′, C5′), 130.8 (d, $^2J_{Cb,Cf\text{-}P}$ = 12 Hz, Cb, Cf), 134.4 (d, $^3J_{Cc,Ce\text{-}P}$ = 10.5 Hz, Cc, Ce), 135.8 (d, $^4J_{Cd\text{-}P}$ = 3 Hz, Cd), 135.8 (C9), 136.4 (C4), 137.8 (C3), 142.4 (C1'), 148.0 (C6), 167.5 (C=O), 201.6 (C=N); HR-ESI-MS, *m/z*: Calcd for $C_{18}H_{14}BrN_2O_6S_3^{2-}$: 530.9177, found 530.9124. Elemental analysis: Found (calculated for $C_{42}H_{34}BrN_2O_6PS_3$): C, 55.65 (58.00); H, 4.04 (3.94) and N, 3.28 (3.22) %.

*2.2.10. Tetraphenylphosphonium (Z)-2-(methoxycarbonyl)-3-(3-nitrophenyl)allyl-(N-4-iodophenylsulfonyl)dithiocarbimate (**2E**)*

Yield = 63%; mp = 76.4–78.1 °C; IR (ATR, cm^{-1}) $\bar{\upsilon}_{max}$ 3079, 2991, 2939, 1712, 1628, 1566, 1529, 1480, 1435, 1364, 1348, 1267, 1207, 1139, 1107, 1081, 996, 947, 814, 782, 755, 725, 686, 597, 557, 523; ^{1}H NMR (300 MHz, $CDCl_3$): δ 3.77 (s, 3H, OCH_3), 4.21 (s, 2H, H1), 7.58–7.68 (m, 14H, Hb, Hf, H3, H8, H2′,H3′, H5′, H6′), 7.72–7.79 (m, 8H, Hc, He), 7.87–7.91 (m, 4H, Hd), 8.09 (d, 2H, $^3J_{5,6} = {}^3J_{6,7}$ = 6 Hz, H7, H9), 8.15 (s, 1H, H5); ^{13}C NMR (75 MHz, $CDCl_3$): δ 33.0 (C1), 52.4 (OCH_3), 97.3 (C4′), 117.4 (d, $^1J_{Ca\text{-}P}$ = 88.5 Hz, Ca), 123.1 (C7), 124.7 (C5), 129.8 (C2′, C6′), 130.2 (C2), 130.7 (C8), 130.8 (d, $^2J_{Cb,Cf\text{-}P}$ = 12.8 Hz, Cb, Cf), 134.4 (d, $^3J_{Cc,Ce\text{-}P}$ = 10.5 Hz, Cc, Ce), 135.8 (d, $^4J_{Cd\text{-}P}$ = 3 Hz, Cd), 135.9 (C9), 136.4 (C4), 136.6 (C3′, C5′), 137.8 (C3), 143.2 (C1'), 148.0 (C6), 167.6 (C=O), 201.5 (C=N); HR-ESI-MS, *m/z*: Calcd for $C_{18}H_{14}IN_2O_6S_3^{2-}$: 576.9064, found 576.8990. Elemental analysis: Found (calculated for $C_{42}H_{34}IN_2O_6PS_3$): C, 53.87 (55.02); H, 3.80 (3.74) and N, 2.99 (3.06) %.

*2.2.11. Tetraphenylphosphonium (Z)-2-(methoxycarbonyl)-3-(2-nitrophenyl)allyl-(N-phenylsulfonyl)dithiocarbimate (**3A**)*

Yield = 90%; mp = 53.4–54.9 °C; IR (ATR, cm^{-1}) $\bar{\upsilon}_{max}$ 3060, 2956, 1712, 1520, 1366, 1276, 1138, 1107, 1079, 943, 825, 564, 523; ^{1}H NMR (300 MHz, $CDCl_3$): δ 3.72 (s, 3H, OCH_3), 4.00 (s, 2H, H1), 7.26–7.28 (m, 3H, H2′, H4′, H6′), 7.44 (*pseudo*-t, 1H, H7), 7.57–7.64 (m, 8H, Hb, Hf), 7.70–7.75 (m, 10H, Hc, He, H8, H9), 7.86–7.90 (m, 7H, Hd, H3, H3′, H5′), 8.04 (d, 1H, $^3J_{6,7}$ = 9 Hz, H6); ^{13}C NMR (75 MHz, $CDCl_3$)**:** δ 33.1 (C1), 52.2 (OCH_3), 117.4 (d, $^1J_{Ca\text{-}P}$ = 89 Hz, Ca), 124.5 (C6), 127.5 (C2′, C6′), 127.8 (C3′, C5′), 129.2 (C7), 129.9 (C4), 130.3 (C4′), 130.7 (C2), 130.7 (d, $^2J_{Cb,Cf\text{-}P}$ = 12.8 Hz, Cb, Cf), 132.1 (C9), 134.4 (d, $^3J_{Cc,Ce\text{-}P}$ = 10.5 Hz, Cc, Ce, C8), 135.8 (d, $^4J_{Cd\text{-}P}$ = 3 Hz, Cd), 137.1 (C3), 143.6 (C1'), 147.3 (C5), 167.3 (C=O), 200.6 (C=N); HR-ESI-MS, *m/z*: Calcd for $C_{18}H_{15}N_2O_6S_3^{2-}$ 451.0092, found 450.9994. Elemental analysis: Found (calculated for $C_{42}H_{35}N_2O_6PS_3$): C, 63.96 (63.78); H, 4.60 (4.46) and N, 3.50 (3.54) %.

*2.2.12. Tetraphenylphosphonium (Z)-2-(methoxycarbonyl)-3-(2-nitrophenyl)allyl-(N-4-fluorophenylsulfonyl)dithiocarbimate (**3B**)*

Yield = 93%; mp = 62.0–63.6 °C; IR (ATR, cm^{-1}) $\bar{\upsilon}_{max}$ 3056, 2948, 1711, 1587, 1518, 1487, 1436, 1341, 1272, 1216, 1138, 1106, 1081, 996, 940, 833, 790, 751, 720, 686, 558, 526, 456; ^{1}H NMR (300 MHz, $CDCl_3$): δ 3.73 (s, 3H, OCH_3), 4.00 (s, 2H, H1), 6.92 (t, 2H, $^3J_{3',2'} = {}^3J_{5',6'} = {}^3J_{3',5',F}$ = 9 Hz, H3′, H5′), 7.43–7.49 (m, 1H, H7), 7.58–7.65 (m, 8H, Hb, Hf), 7.68–7.79 (m, 10H, Hc, He, H8, H9), 7.87–7.94 (m, 7H, Hd, H3, H2′, H6′), 8.06 (d, 1H, $^3J_{6,7}$ = 9 Hz, H6); ^{13}C NMR (75 MHz, $CDCl_3$): δ 33.1 (C1), 52.2 (OCH_3), 114.3 (d, $^2J_{C3',C5'\text{-}F}$ = 22.5 Hz, C3′,C5′), 117.4 (d, $^1J_{Ca\text{-}P}$ = 89 Hz, Ca), 124.5 (C6), 129.2 (C7), 129.8 (C4), 130.5 (d, $^3J_{C2',C6'\text{-}F}$ = 9 Hz, C2′,C6′), 130.7 (C2), 130.8 (d, $^2J_{Cb,Cf\text{-}P}$ = 12.8 Hz, Cb, Cf), 132.0 (C9), 134.3 (C8), 134.4 (d, $^3J_{Cc,Ce\text{-}P}$ = 10.5 Hz, Cc, Ce), 135.8 (d, $^4J_{Cd\text{-}P}$ = 3 Hz, Cd), 137.2 (C3), 139.6 (d, $^4J_{C1'\text{-}F}$ = 3 Hz, C1′), 147.4 (C5), 163.8 (d, $^1J_{C4'\text{-}F}$ = 247.5 Hz, C4′), 167.3 (C=O), 201.1 (C=N); HR-ESI-MS, *m/z*: Calcd for $C_{18}H_{14}FN_2O_6S_3^{2-}$: 469.0004, found 469.0037. Elemental analysis: Found (calculated for $C_{42}H_{34}FN_2O_6PS_3$): C, 61.25 (62.36); H, 4.38 (4.24) and N, 3.50 (3.46) %.

*2.2.13. Tetraphenylphosphonium (Z)-2-(methoxycarbonyl)-3-(2-nitrophenyl)allyl-(N-4-chlorophenylsulfonyl)dithiocarbimate (**3C**)*

Yield = 97%; mp = 57.4–58.9 °C; IR (ATR, cm^{-1}) $\bar{\upsilon}_{max}$ 3060, 2950, 1712, 1637, 1610, 1575, 1518, 1483, 1470, 1436, 1369, 1340, 1265, 1207, 1137, 1107, 1081, 1009, 996, 948, 859, 816, 790, 752, 721, 690, 673, 605, 559, 524, 413; ^{1}H NMR (300 MHz, $CDCl_3$): δ 3.74 (s, 3H, OCH_3), 4.00 (s, 2H, H1), 7.21 (d, 2H, $^3J_{3',2'} = {}^3J_{5',6'}$ = 9 Hz, H2′, H6′), 7.43–7.50 (m, 1H, H7), 7.57–7.68 (m, 10H, Hb, Hf, H8, H9), 7.72–7.78 (m, 8H, Hc, He), 7.82–7.91 (m, 7H, Hd, H3, H3′, H5′), 8.06 (d, 1H, $^3J_{6,7}$ = 9 Hz, H6); ^{13}C NMR (75 MHz, $CDCl_3$): δ 33.1 (C1), 52.3 (OCH_3), 117.4 (d, $^1J_{Ca\text{-}P}$ = 89 Hz, Ca), 124.6 (C6), 127.6 (C2′, C6′), 129.2 (C7), 129.5 (C3′, C5′), 129.8 (C4), 130.7 (d, $^2J_{Cb,Cf\text{-}P}$ = 12.8 Hz, Cb, Cf), 130.8 (C2), 132.0 (C9), 134.3 (C8), 134.4 (d, $^3J_{Cc,Ce\text{-}P}$ = 10.5 Hz, Cc, Ce), 135.8 (d, $^4J_{Cd\text{-}P}$ = 3 Hz, Cd), 136.3 (C4′), 137.3 (C3), 142.1 (C1'), 147.3 (C5), 167.3 (C=O), 201.5 (C=N); HR-ESI-MS, *m/z*: Calcd for $C_{18}H_{14}ClN_2O_6S_3^{2-}$: 484.9708, found 484.9747. Elemental analysis: Found (calculated for $C_{42}H_{34}ClN_2O_6PS_3$): C, 57.62 (61.12); H, 4.14 (4.15) and N, 3.54 (3.39) %.

*2.2.14. Tetraphenylphosphonium (Z)-2-(methoxycarbonyl)-3-(2-nitrophenyl)allyl-(N-4-bromophenylsulfonyl)dithiocarbimate (**3D**)*

Yield = 96%; mp = 60.4–62.0 °C; IR (ATR, cm^{-1}) $\bar{\upsilon}_{max}$ 3068, 2989, 1715, 1649, 1605, 1571, 1518, 1484, 1471, 1435, 1367, 1343, 1267, 1205, 1141, 1106, 1080, 1010, 948, 862, 817, 750, 738, 720, 689, 674, 604, 558, 525, 458, 415; ^{1}H NMR (300 MHz, $CDCl_3$): δ 3.73 (s, 3H, OCH_3), 3.99 (s, 2H, H1), 7.37 (d, 2H, $^3J_{3',2'} = {}^3J_{5',6'}$ = 9 Hz, H2′, H6′), 7.42–7.51 (m, 1 H, H7), 7.57–7.64 (m, 10H, Hb, Hf, H8, H9), 7.69–7.81 (m, 10H, Hc, He, H3′, H5′), 7.85–7.93 (m, 5H, Hd, H3), 8.06 (d, 1H, $^3J_{6,7}$ = 9 Hz, H6); ^{13}C NMR (75 MHz, $CDCl_3$): δ 33.1 (C1), 52.3 (OCH_3), 117.4 (d, $^1J_{Ca\text{-}P}$ = 89 Hz, Ca), 124.6 (C6), 124.9 (C4′), 129.2 (C7), 129.7 (C2′, C6′), 129.7 (C4), 130.6 (C2), 130.7 (d, $^2J_{Cb,Cf\text{-}P}$ = 13.5 Hz, Cb, Cf), 131.9 (C9), 134.3 (C3′, C5′), 134.4 (d, $^3J_{Cc,Ce\text{-}P}$ = 10.5 Hz, Cc, Ce), 135.8 (d, $^4J_{Cd\text{-}P}$ = 3 Hz, Cd), 135.8 (C8), 137.4 (C3), 142.5 (C1'), 147.3 (C5), 167.3 (C=O), 201.6 (C=N); HR-ESI-MS, *m/z*: Calcd for $C_{18}H_{14}BrN_2O_6S_3^{2-}$: 530.9177, found 530.9147. Elemental analysis: Found (calculated for $C_{42}H_{34}BrN_2O_6PS_3$): C, 54.97 (58.00); H, 3.86 (3.94) and N, 3.51 (3.22) %.

*2.2.15. Tetraphenylphosphonium (Z)-2-(methoxycarbonyl)-3-(2-nitrophenyl)allyl-(N-4-iodophenylsulfonyl)dithiocarbimate (**3E**)*

Yield = 97%; mp = 62.6–64.2 °C; IR (ATR, cm^{-1}) $\bar{\upsilon}_{max}$ 3066, 3048, 1713, 1650, 1604, 1567, 1518, 1481, 1436, 1367, 1342, 1278, 1264, 1206, 1170, 1142, 1106, 1079, 1004, 947, 862, 811, 782, 752, 720, 690, 600, 558, 526, 456; ^{1}H NMR (300 MHz, $CDCl_3$): δ 3.73 (s, 3H, OCH_3), 3.99 (s, 2H, H1), 7.43–7.48 (m, 1H, H7), 7.57–7.67 (m, 14H, Hb, Hf, H8, H9, H2′, H3′, H5′, H6′), 7.70–7.81 (m, 8H, Hc, He), 7.87–7.91 (m, 5H, Hd, H3), 8.06 (d, 1H, $^3J_{6,7}$ = 9 Hz, H6); ^{13}C NMR (75 MHz, $CDCl_3$): δ 33.1 (C1), 52.3 (OCH_3), 97.3 (C4′), 117.4 (d, $^1J_{Ca\text{-}P}$ = 89 Hz, Ca), 124.6 (C6), 129.3 (C7), 129.7 (C2′, C6′), 129.7 (C4), 130.7 (d, $^2J_{Cb,Cf\text{-}P}$ = 12,8 Hz, Cb, Cf), 130.8 (C2), 131.9 (C9), 134.3 (C8), 134.4 (d, $^3J_{Cc,Ce\text{-}P}$ = 10.5 Hz, Cc, Ce), 135.8 (d, $^4J_{Cd\text{-}P}$ = 3 Hz, Cd), 136.6 (C3′, C5′), 137.4 (C3), 143.2 (C1'), 147.3 (C5), 167.2 (C=O), 201.5 (C=N); HR-ESI-MS, *m/z*: Calcd for $C_{18}H_{14}IN_2O_6S_3^{2-}$: 576.9064, found 576.9019. Elemental analysis: Found (calculated for $C_{42}H_{34}IN_2O_6PS_3$): C, 53.27 (55.02); H, 3.77 (3.74) and N, 3.03 (3.06) %.

2.3. X-ray crystallography

Slow evaporation of ethanol/water solution (1:1 v/v) of compound **1A**, or acetone/water solutions (1:1 v/v) of **2A** and **3A** at 298 K yielded yellow crystals. The diffraction pattern of **1A** was collected at room temperature on a Bruker APEXII-CCD diffractometer using Cu-Kα radiation (λ = 1.54178 Å) monochromated by graphite. The software APEX2 [19] was employed to operate the diffractometer and to plan the data collection strategy. The data were integrated using the program SAINT [20]. TWINABS-2012/1 [21] was used for absorption correction. Using Olex2 [22], the structure was solved with the Olex2.solve structure solution program [23] using Charge Flipping and refined with the SHELXL-2018 [24]. Compound **1A** was refined as a merohedral twin with twin matrix (−1, 0, 0; 0, −1, 0; 0, 0, 1), with a refined BASF value of 0.40899. All hydrogen atoms were stereochemically positioned and refined with the riding model. Some of the aromatic carbon atoms of the tetraphenylphosphonium cation of **1A** presented

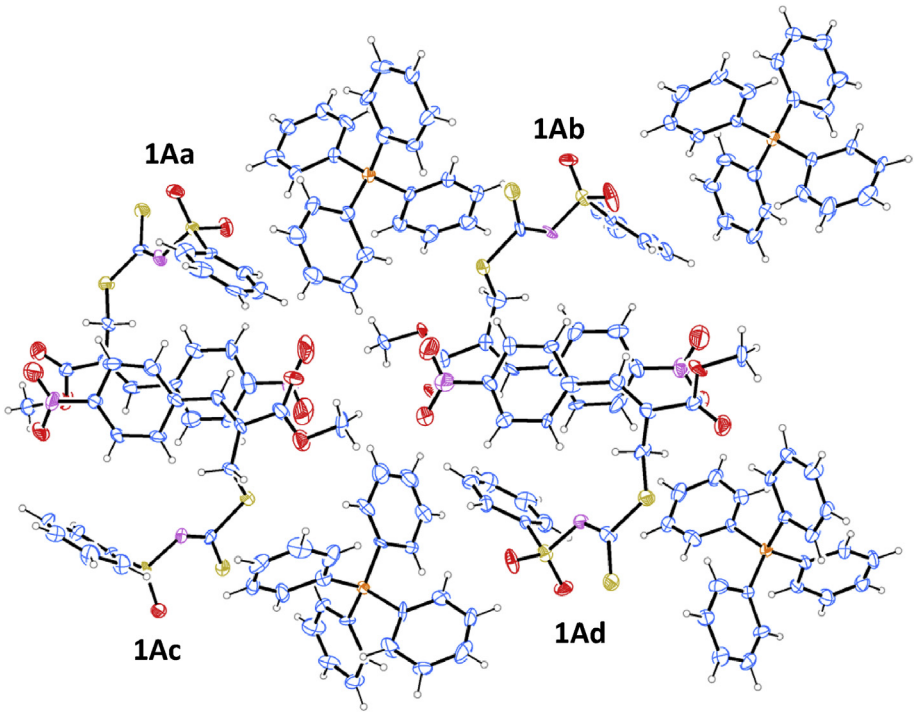

Fig. 2. ORTEP representation of the four cations and four anions of the asymmetric unit of **1A**.

uncharacteristically large and irregular thermal parameters compared to those of **2A** and **3A**, and were constrained using SIMU in SHELXL-2018 [24].

The X-ray intensity data for compounds **2A** and **3A** single crystals were collected on a Bruker AXS Proteum X8 diffractometer using Mo-Kα radiation (λ = 0.71073 Å) monochromated by graphite. The software APEX2 [19] was employed to operate the diffractometer and to plan the data collection strategy. The data were integrated using the program SAINT [20], and corrected for absorption effects using multi-scan and scaled with the program SADABS [25]. The structures were solved by direct methods and refined by full-matrix least-square methods against F^2, with SHELXL-2018 [24]. All hydrogen atoms were stereochemically positioned and refined with the riding model. In the compound **3A**, the O6 atom of the anion was found to have uncharacteristically large and irregular thermal parameters compared to other oxygen atoms of the structure and were constrained using SIMU in SHELXL-2018 [24].

Structural representations were drawn using ORTEP-3 [26] and MERCURY [27]. The program WinGX [26] was used to prepare materials for publication. Table 1 summarizes the data collection and experimental details for the salts **1A**, **2A** and **3A**.

2.4. Hirshfeld surface (HS)

The Hirshfeld 3D surfaces were generated with the Crystal Explorer 2.1 program [28]. The strength of the interactions were calculated by Hirshfeld *d*norm (normalized contact distance) surface. Moreover, the 2D fingerprint plots were calculated in order to analyze the relative contribution of different intermolecular interactions of compounds **1A**, **2A** and **3A**. The 3D *d*norm surface was mapped using a fixed color scale of −0.1000 (red) to 1.0000 (blue). Although the compound **1A** crystal is twin and present four cations and four anions in the asymmetric unit, *d*norm was generated for only one set of cation and anion. The 2D fingerprint plots were displayed on the graph axes (0.4–3.0 Å), using *de* and *di* distance scales. The molecular electrostatic potentials on Hirshfeld surfaces of the anion were mapped using a fixed scale of −0.04 to 0.03 au for **1A**, **2A** and **3A**. All hydrogen bond lengths were automatically modified to typical standard neutron values (C—H of 1.083 Å).

2.5. Biological assays

The biological activity of the allyldithiocarbimate salts was evaluated *in vitro* through the *Poisoned Food* method [29]. For the initial screening with *Botrytis cinerea*, *Rhizoctonia solani*, *Sclerotinia sclerotiorum*, *Alternaria solani*, *Colletotrichum acutatum* and *Fusarium oxysporum*, the potato dextrose agar culture medium (PDA, 2.34 g) was mixed with dimethyl sulfoxide (DMSO, 0,60 mL), polyoxyethylene (20) sorbitan monooleate (Tween 80, 0,60 mL), the compound **1C** (7.92 mg, for a final concentration of 160 μM) and distilled water for a final volume of 60,0 mL. This mixture was distributed in four Petri dishes per treatment. The control (Four repetitions for each fungus) was prepared with PDA, DMSO, Tween 80 and water only. Each dish was inoculated with one disc of mycelia (7.4 mm). The dishes were kept under controlled temperature until the fungus colony had taken 90% of the dish area on the control dishes: three days at 20 °C for *B. cinerea*, *R. solani* and *S. slerotiorum*, four days at 25 °C for *A. solani* or seven days at 25 °C for *C. acutatum* and *F. oxysporum*. The mycelial growth was calculated from the average of the diameters measured in six directions in each Petri dish, in the last day of each experiment. The inhibition percentage (I%) of the mycelial growth was calculated with the equation: I% = 100 x (C − S)/C, where C is the average growth of the control and S is the average growth of the fungus in the presence of the substance in test. As *B. cinerea* showed the highest sensitivity to the allyldithiocarbimate salt **1C,** the test was repeated with this fungus including treatments with the substances **1A-E**, **2A-E** and **3A-E** at various concentrations (5, 10, 20, 40, 120, and 160 μM). From these data, dose-response curves were plotted, and the concentration required to inhibit the mycelial growth of *B. cinerea* by 50% (IC_{50}) was determined for each substance.

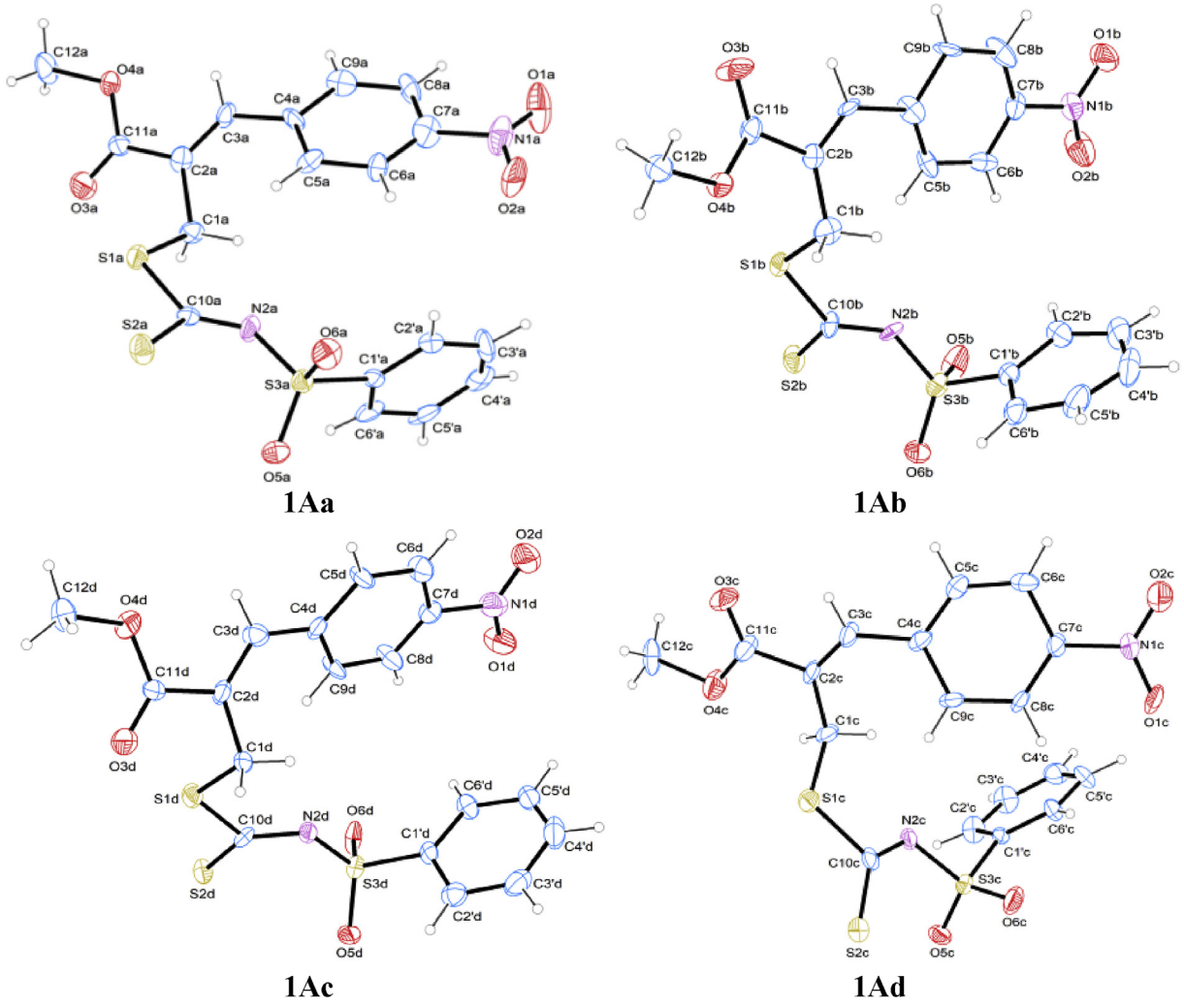

Fig. 3. ORTEP views of the four anions of the asymmetric unit of **1A** with atom-numbering scheme and displacement ellipsoids drawn with 30% probability level.

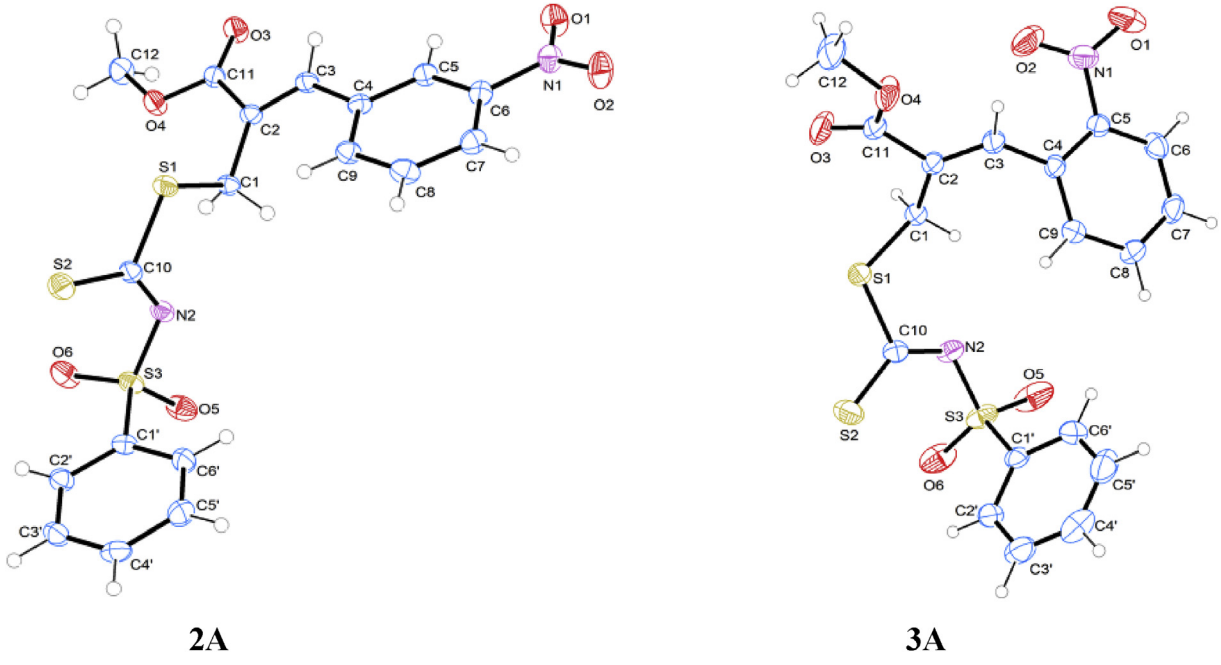

Fig. 4. ORTEP views of the anions of **2A** and **3A** with atom-numbering scheme and displacement ellipsoids drawn with 30% probability level.

Table 2
Selected geometrical parameters for compounds **1A**, **2A** and **3A**.

Compound	**1A**[a]	**2A**	**3A**
Bond length (Å)			
C1–C2	1.50(2)	1.498(3)	1.503(3)
C2–C3	1.31(2)	1.342(4)	1.334(3)
C3–C4	1.50(2)	1.462(4)	1.477(3)
C2–C11	1.50(2)	1.498(4)	1.489(3)
C11–O4	1.33(2)	1.332(3)	1.329(3)
C11–O3	1.19(2)	1.201(3)	1.196(3)
C12–O4	1.48(2)	1.455(3)	1.445(3)
C1–S1	1.82(1)	1.813(3)	1.830(2)
C10–S1	1.78(1)	1.772(3)	1.776(2)
C10–N2	1.32(2)	1.318(4)	1.316(3)
C10–S2	1.68(1)	1.675(3)	1.680(3)
N2–S3	1.62(1)	1.617(2)	1.623(2)
S3–C1′	1.75(1)	1.768(3)	1.772(3)
Torsion angles			
N2–S3–C1′–C2′	103.49	129.3(2)	109.5(2)
N2–S3–C1′–C6′	−75.49	−54.1(2)	−71.1(2)
S1–C1–C2–C3	116.98	−91.5(3)	−56.5(3)
S1–C1–C2–C11	−73.77	93.1(3)	132.0(2)

[a] Values of the average bond lengths of the four molecules of the asymmetric unit (**1Aa-d**) and torsion angles of the anion of **1Aa**.

3. Results and discussion

3.1. Syntheses

Scheme 1 shows the preparation of the key starting materials for the synthetic route. The five dihydrated potassium *N*-R-sulfonyldithiocarbimates with the general formula $K_2(R\text{-}SO_2N{=}CS_2)\cdot 2H_2O$, where R = C_6H_5, 4-FC_6H_4, 4-ClC_6H_4, 4-BrC_6H_4 and 4-IC_6H_4, are yellow salts, soluble in water and insoluble in most organic solvents. Their infrared spectra were in accordance with the reported data [9–14]. Three Morita-Baylis-Hillman adducts were prepared by the reactions of *p*-, *m*- and *o*-nitrobenzaldehydes with methyl acrylate in the presence of DABCO as catalyst (Scheme 1) [15]. These compounds were converted into allylic bromides in reaction with lithium bromide and sulfuric acid in acetonitrile (Scheme 1) [16]. After purification by column chromatography, the infrared and NMR spectroscopic data of the Morita-Baylis-Hillman adducts [15] and the allylic bromides reproduced the literature values [16–18].

Scheme 2 shows the syntheses of the new compounds **1A-E**, **2A-E** and **3A-E**. As the *N*-R-sulfonyldithiocarbimates are dianionic species, a slight excess of these nucleophiles and the slow addition of the allylic bromides to the reacting system avoided a second substitution reaction at the free sulfur atom of the allyldithiocarbimate monoanion thus formed. These substitution reactions are quite fast (less than 15 minutes). The allyldithiocarbimate potassium salts are very soluble in water and of difficult purification. Thus, the new allyldithiocarbimates were isolated in high yields (89% average) as tetraphenylphosphonium salts (Scheme 2).

Compounds **1A-E**, **2A-E** and **3A-E** are yellow solids soluble in chloroform, dimethylformamide, dimethyl sulfoxide, acetonitrile, dichloromethane, acetone, ethyl acetate and methanol, and are practically insoluble in water, hexane and diethyl ether. The melting point ranges of compounds **1A-E** (with the *para*-nitro group) are higher than the values observed for the corresponding analogues **2A-E** (with the *meta*-nitro group). Although solids at room temperature, the **3A-E** series (with the *ortho*-nitro group) presented the lowest melting points, in the range of 53–64 °C, characteristic of ionic liquids.

3.2. Spectroscopic characterization

HR-ESI-MS in the anionic mode showed the expected values for the $[M]^-$ peaks, thus confirming the allyldithiocarbimate anions formulae. The molecular peak of tetraphenylphosphonium cation was observed in the positive mode at m/*z* 339.1353.

The IR spectra of compounds **1A-E**, **2A-E** and **3A-E** showed the asymmetric and symmetric stretching bands of the NO_2 group at 1514–1529 and 1340–1353 cm^{-1}, respectively, as well as the intense band in 1705–1725 cm^{-1}, attributed to νC=O of the ester group. The most important bands to characterize the dithiocarbimate moiety were identified at 1340–1384 cm^{-1} (νC=N) and 933–948 cm^{-1} ($\nu_{asym}CS_2$). In the spectra of the parent potassium *N*-R-sulfonyldithiocarbimates, these bands are observed at 1249–1255 and 962–970 cm^{-1}, respectively. These data indicated an increase in the C=N double bond character with the transformation of the free dianion (dithiocarbimate) into the monoanion (allyldithiocarbimate), with a less conjugated NCS_2 system. The $\nu_{asym}SO_2$ and $\nu_{sym}SO_2$ bands were observed in the expected ranges of 1256–1276 and 1133–1142 cm^{-1} in the spectra of **1A-E**, **2A-E** and **3A-E**.

In their ^1H NMR spectra, the tetraphenylphosphonium cation signals are observed as multiplets at similar chemical shifts, at about δ 7.6–7.7 (Hb and Hf), 7.7–7.8 (Hc and He) and 7.9 (Hd). In most spectra, these signals overlap with those of other aromatic hydrogens of the anions. The integration curves are consistent with the number of hydrogens present in the structures of **1A-E**, **2A-E** and **3A-E** and confirmed the 1:1 proportion between the cation and the anions. The singlets at δ 3.72–3.78 and 3.99–4.22 confirmed

Table 3
Hydrogen-bond geometry (Å, °) for compounds **1Aa, 2A** and **3A**.

Donor–H···Acceptor	d(D–H)	d(H···A)	d(D···A)	<(DHA)
Compound **1A**[a]				
C2′a–H2′a···O6a	0.93	2.49	2.85(2)	103
C1a–H2′A···N2a	0.97	2.44	2.94(2)	111
C3a–H3a···O4a	0.93	2.28	2.67(2)	105
C23a–H23a···S3a	0.93	2.94	3.81(1)	155
C23a–H23a···O5a	0.93	2.67	3.60(2)	175
C5′a–H5′a···O6a^{i}	0.93	2.35	3.17(2)	147
C5′c–H5′c···O4a^{i}	0.93	2.67	3.29(2)	125
C12d–H12I···O3a^{ii}	0.96	2.70	3.54(2)	147
C14b–H14b···S2a^{iii}	0.93	2.93	3.53(2)	123
C17a–H17a···S2d^{iv}	0.93	2.84	3.54(2)	134
C26b–H26b···O3a^{iii}	0.93	2.71	3.32(2)	124
C27b–H27b···O3a^{iii}	0.93	2.71	3.31(2)	123
C33d–H33d···S2a^{v}	0.93	2.90	3.58(2)	131
C22a–H22a···π1^{vi}	0.93	2.74	3.66(2)	173
Compound **2A**				
C2′–H2′···O6	0.93	2.51	2.8963(3)	105
C3–H3···O3	0.93	2.35	2.7538(2)	106
C9–H9···S1	0.93	2.76	3.6051(3)	151
C17–H17···O2	0.93	2.46	3.1231(3)	129
C1–H1A···π2	0.97	2.81	3.5801(3)	137
C4′–H4′···O3^{vii}	0.93	2.41	3.2517(3)	151
C8–H8···O6^{viii}	0.93	2.40	3.0968(3)	132
C18–H18···O5^{iii}	0.93	2.60	3.3416(3)	137
C30–H30···O1^{viii}	0.93	2.37	3.2909(3)	170
C35–H35···S2^{i}	0.93	2.86	3.4753(3)	125
C27–H27···π4^{ix}	0.93	2.77	3.5610(3)	144
C29–H29···π3^{x}	0.93	2.94	3.6305(3)	132
C34–H34···π3^{xi}	0.93	2.76	3.5437(3)	143
Compound **3A**				
C2′–H2′···O6	0.93	2.59	2.9551(1)	104
C1–H1B···N2	0.97	2.42	2.9530(1)	115
C3–H3···O4	0.93	2.34	2.7182(1)	104
C33–H33···O5	0.93	2.74	3.148(4)	107
C28–H28···O3^{xii}	0.93	2.70	3.340(3)	127
C29–H29···O6^{xiii}	0.93	2.60	3.3457(1)	138
C36–H36···O2^{xiv}	0.93	2.58	3.2307(1)	128

Symmetry codes: (i) 1+x,y,z; (ii) 1+x,y,1+z; (iii) x,y,1+z; (iv) 2-x,-1/2+y,1-z; (v) -x,1/2+y,1-z; (vi) −1+x,y,z; (vii) 1-x,1-y,1-z; (viii) 1-x,2-y,2-z; (ix) 1-x,1-y,-z; (x) -x,-y,-z; (xi) 1-x,1-y,1-z; (xii) 1-x,-y,1-z; (xiii) -x,1-y,-z; (xiv) 1-x,y, 1/2-z. π1 is ring C31d to C36d, π2 is ring C13 to C18, π3 is ring C1′ to C6′ and π4 is ring C19 to C24.
[a] Interactions related to **1Aa**.

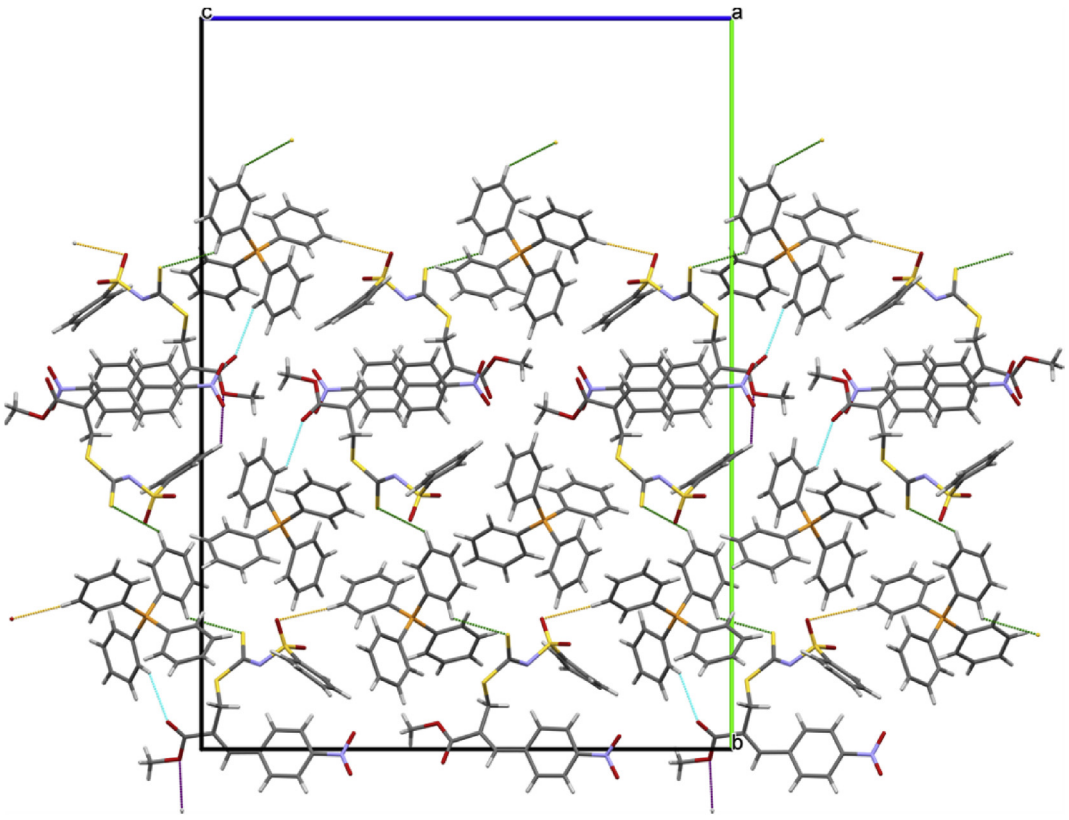

Fig. 5. Packing diagram of **1A**, viewed down the *c* axis. Dashed lines indicate C–H···O and C–H···S intermolecular interactions.

the presence of the methoxy group and the methylene hydrogens (H1), respectively, in the allyldithiocarbimates structures.

The methoxy and the methylene (C1) carbon atoms signals are observed in their ^{13}C NMR spectra, respectively, at δ 52.2–52.9 and δ 32.0–33.5. The ester carbonyl signal appears at the expected range of *ca.* δ 167. It is interesting to note that the C=N signal (*ca.* δ 200) is observed in higher field when compared to the corresponding signal observed in the spectra of the parent potassium *N*-R-sulfonyldithiocarbimates (*ca.* δ 225) [29]. Thus, the NMR and the IR data are strongly influenced by the increase of the C=N double bond character in the allyldithiocarbimates.

The ^{13}C NMR signals of the tetraphenylphosphonium cation appeared as doublets with the expected *J* values in the spectra of **1A**-**E**, **2A**-**E** and **3A**-**E**, due to coupling with the phosphorus atom: 89 Hz for Ca, 13 Hz for Cb and Cf, 10 Hz for Cc and Ce, and 3 Hz for Cd.

3.3. X-ray crystallography

To gain a deeper insight into the structures of the allyldithiocarbimates, we decided to investigate one compound of each series by X-ray crystallography. After several crystallization attempts, we managed to obtain suitable crystals of compounds **1A** from ethanol/water solutions (1:1 v/v), **2A** and **3A** from acetone/water solutions (1:1 v/v). These compounds presented the nitro group in *para*, *meta* and *ortho* positions, respectively (Scheme 2).

The X-ray data showed that compound **1A** crystallizes in the non-centrosymmetric space group $P2_1$ of the monoclinic system, while **2A** crystallizes in the centrosymmetric space group $P\bar{1}$ of the triclinic system and **3A** in the space group P2/c of the monoclinic system. Four anions and four cations form the asymmetric unit of compound **1A** (Fig. 2), whereas the asymmetric units of compounds **2A** and **3A** contain only one anion and one cation.

The four anions present in compound **1A** crystal (**1Aa**, **1Ab**, **1Ac**, **1Ad**) are shown separately in Fig. 3, for clarity. In this picture, it is possible to see that the anions are present in different conformations. The X-ray diffraction data of compounds **1A**, **2A** and **3A** confirmed the (*Z*)-stereochemistry for the allyldithiocarbimate anions (Figs. 3 and 4).

Table 2 presents selected bond lengths and torsion angles for the anions of **1A** (average values of the four anions), **2A** and **3A**. There are four planar fragments in these anions: C1–S1–C10–S2–N2–S3, C1–C2–C3–C4–C11 and the two aromatic rings. In all compounds, the torsion angles around the bonds S3–C1' and C1–C2 showed different conformations of these three last fragments in relation to the least square plan through the C1–S1–C10–S2–N2–S3 atoms (Table 2).

The distances in the methoxycarbonyl group are within the reported range for related compounds [6,30–32]. The bond length C2–C3 is consistent with a typical C=C double bond [33]. The C3–C4 and C2–C11 distances are shorter than a normal C–C single bond of *ca.* 1.54 Å [33]. These values are similar to those reported for related compounds [6]. The C10–N2 distances have a partial double bond character and are shorter than those observed in the free ligands. For example, the C10–N2 distance for the potassium *N*-4-iodophenylsulfonyldithiocarbimate is 1.342(9) Å [11].

The C1–S1 distances are slightly longer than typical C–S single bonds in all compounds. The C10–S1 and C1′–S3 distances are shorter than a C–S single bond and the C10–S2 is longer than a typical C=S double bond [33]. This fact is due to the conjugated character of the NCS_2 system and is observed in the structures of other allyldithiocarbimates [6] and disulfides derived from sulfonyldithiocarbimates [30]. These observations agree with the spectroscopic data.

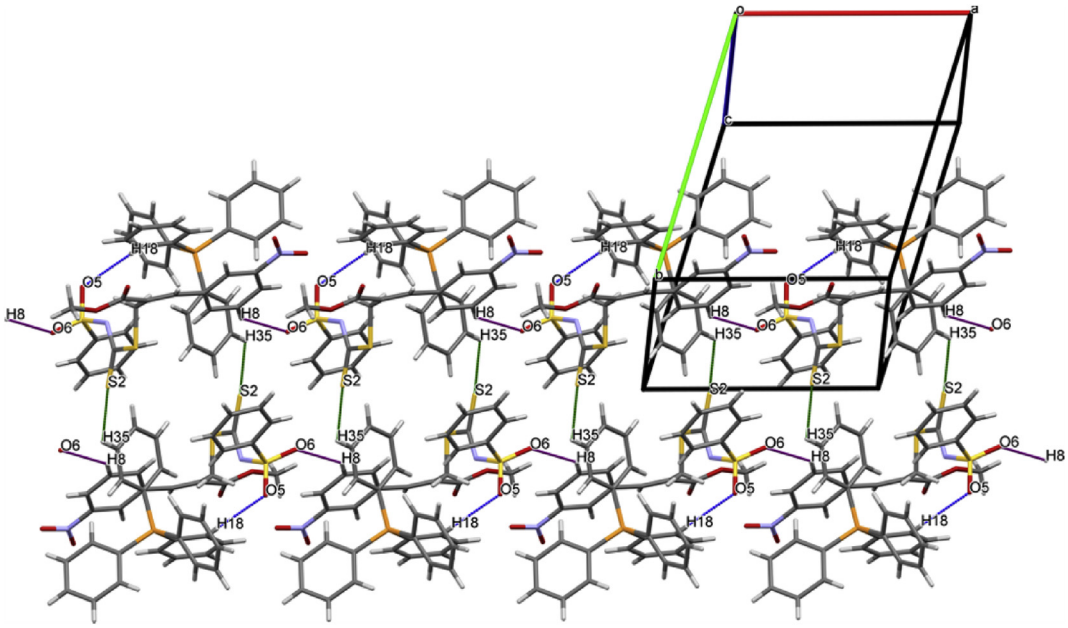

Fig. 6. Packing diagram of **2A**, viewed down the *a* axis. Dashed lines indicate C—H···O and C—H···S intermolecular interactions.

The bond lengths and angles in the tetraphenylphosphonium cation are within the reported range [6,30]. The phosphorus atom present tetrahedral distorted geometry with the C—C bond lengths and the C—P—C angles in the four phenyl rings ranging from 1.28(2) Å to 1.47(2) Å and from 104.1(2) to 114.3(6)°, respectively. In compound **3A,** the phosphorus atom is in a special position (0,y, 1/4).

The crystal packings in **1A**, **2A** and **3A** are stabilized mainly by electrostatic interactions between oppositely charged ions. C—H···O intramolecular interactions are observed in the three compounds. Other intramolecular interactions are particular to some crystals such as C—H···N (compounds **1A** and **3A**), C—H···S (compounds **1A** and **2A**) and C—H···π (compound **2A**). In addition, the three compounds present contacts between cations and anions: C—H···O in all compounds, C—H···S (compound **1A**) and C—H···π (compound **1A** and **2A**). The geometric parameters of these interactions are listed in Table 3.

In compound **1A**, the C26b—H26b···O3a and C27b—H27b···O3a intermolecular interactions form dimmers, generating $R_2^1(5)$ ring motifs [34]. The C—H···O (between anions) and C—H···S (between cations and anions) intermolecular interactions form chains which are interlinked by C—H···π giving rise to a supramolecular network (Fig. 5).

In compound **2A**, the C8—H8···O6 interactions between anions and the C18—H18···O5 contacts between cations and anions form ribbons along the *a* axis which are interlinked by C—H···S and C30—H30···O1 intermolecular interactions forming bidimensional layers. These layers are linked by C4′—H4′···O3 hydrogen bonds along the *a* axis. Moreover, there are three C—H···π intermolecular interactions between cations and anions stabilizing the three-dimensional arrangement (Fig. 6).

In compound **3A**, the C28—H28···O3 and C36—H36···O2 intermolecular interactions between cations and anions form zigzag chains along the *c* axis, which are connected by C29—H29···O6 hydrogen bonds in the *a* axis direction giving rise to a three-dimensional network (Fig. 7).

3.4. Hirshfeld surface

The molecular electrostatic potentials mapped (Fig. 8) on Hirshfeld surfaces of the anions were calculated over the −0.04 to 0.03 au range for **1Aa**, **2A** and **3A**. Specifically, the blue (electropositive) and red (electronegative) mapping provided a special insight on the electronic delocalization that occurs in compound **3A** due to the presence of the nitro group in *ortho* position, which is not observed in compound **2A** where the nitro group is in the *meta* position. It is possible to observe in compound **2A** a dark blue area between the nitro group and the ester carbonyl, whereas in compound **3A** there is a small white area between these groups, indicating a decrease in polarity. Moreover, in **1Aa,** where the nitro substituent is in *para* position, a larger blue area is observed between the nitro and the carbonyl groups. Considering the greater distance between these groups in **1Aa,** an even higher polarity is expected. These differences partially explain the melting point decrease from **1A** to **2A** and **3A** (156.9 °C > 136.4 °C > 53.4 °C, respectively), as the increase in the polarity of the anion favors the intermolecular interactions. The small number of strong interactions present in the crystalline packaging of **3A** (Table 3) explains its ionic liquid behavior.

In order to visualize the importance of intermolecular interactions in the crystal structures of **1A**, **2A** and **3A,** HS analyses were carried out to investigate the atom···atom interactions. The HS mapped with d_{norm} for these compounds highlighted stronger interactions in the brightest red areas (Fig. 9), indicating both acceptors and donors. They correspond mainly to strong C—H···O hydrogen bonds, showing their significant participation in the crystal structure.

The 2D fingerprint plots are useful to identify particular atom pair close contacts and show the relative contribution of different intermolecular interactions to the Hirshfeld surface. Thus, Fig. 10 illustrates a summary of selected percentages of the intermolecular interactions contributions for the crystal structures of **1A**, **2A** and **3A.** This analysis shows that H···H, C···H, H···C, O···H and H···O, S···H and H···S contacts determine the crystals packings. All interactions show a similar pattern, except for the H···O and H···S contacts, which have different values in all structures. The non-

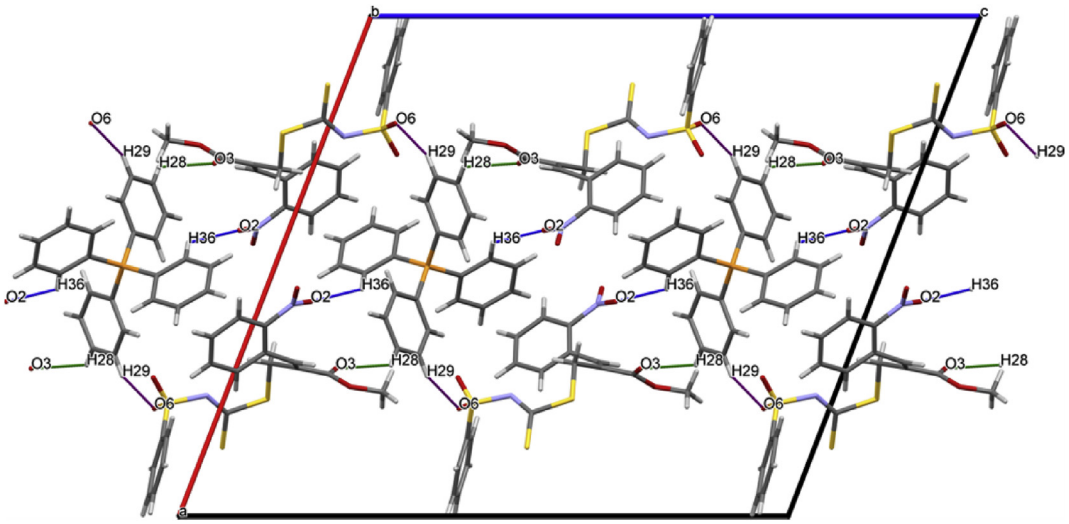

Fig. 7. Packing diagram of **3A**, viewed down the *c* axis. Dashed lines indicate C—H···O intermolecular interactions.

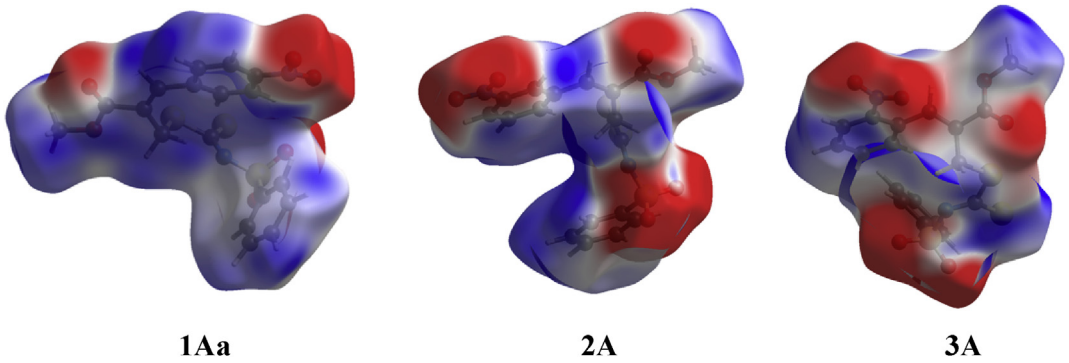

Fig. 8. Electrostatic potential mapping of the anions of **1Aa**, **2A** and **3A**.

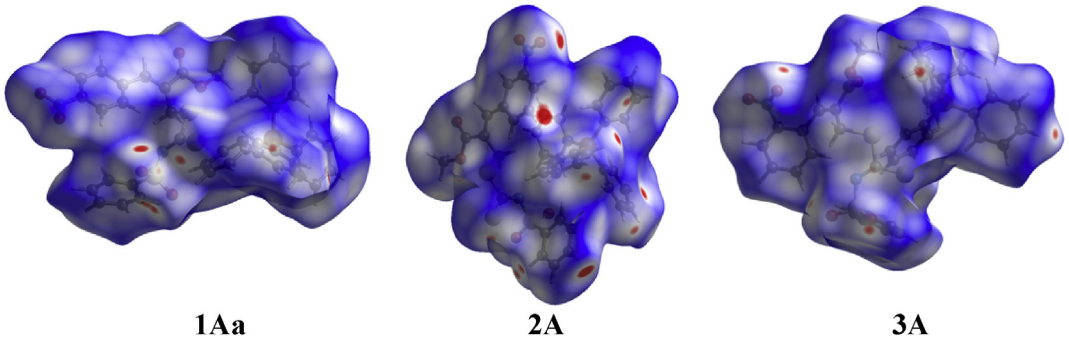

Fig. 9. View of the three-dimensional Hirshfeld surfaces plotted over d_{norm} of **1Aa**, **2A** and **3A**, respectively. The surfaces are partially transparent for clarity.

classical H···H interactions are the main contributors to the total Hirshfield surface (42.7% in **1A** and *ca.* 39% in **2A** and **3A**, Fig. 11). The C···H/H···C contributions for the crystal packagings (21.6% in **1A**, 24.3% in **2A**, and 25.5% in **3A**) are also important. No significant π···π interactions were found within the crystals (the C···C contacts make only 2.8%, 1.9% and 0.7% of the surface area, respectively for **1A**, **2A** and **3A**).

3.5. Biological tests

Biological tests with six fungi species (*B. cinerea*, *C. acutatum*, *A. solani*, *R. solani*, *F. oxysporum* and *S. sclerotiorum*) were carried out in order to evaluate the agrochemical potential of the new allyldithiocarbimate salts. These microorganisms belong to various families and were chosen due to the enormous losses they can cause in economically important crops. The gray mold disease caused by *B. cinerea* affects more than 200 host plants in different stages of development and several tissues (shoots, fruits, flowers, leaves and storage organs), being one of the most important postharvest decays of fruits and vegetables [3,35]. *C. acutatum* is also a fungus with a broad host range, being very destructive in olives and strawberry crops, for example. It can cause anthracnose and other plant

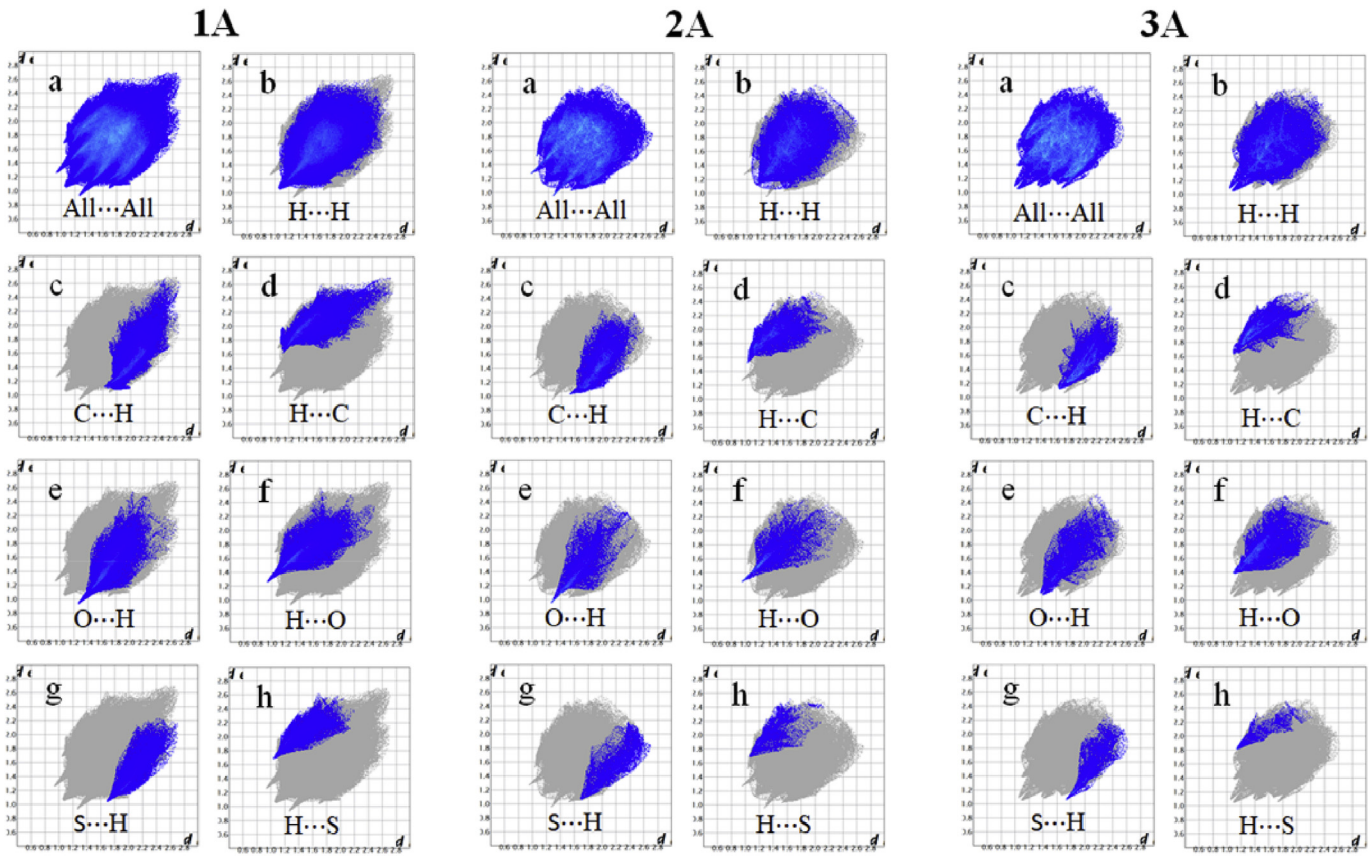

Fig. 10. Two-dimensional fingerprint plots for compounds **1A** (a–h), **2A** (a–h) and **3A** (a–h). The *di* and *de* values are the closest internal and external distances (in Å) from given points on the Hirshfeld surface contacts.

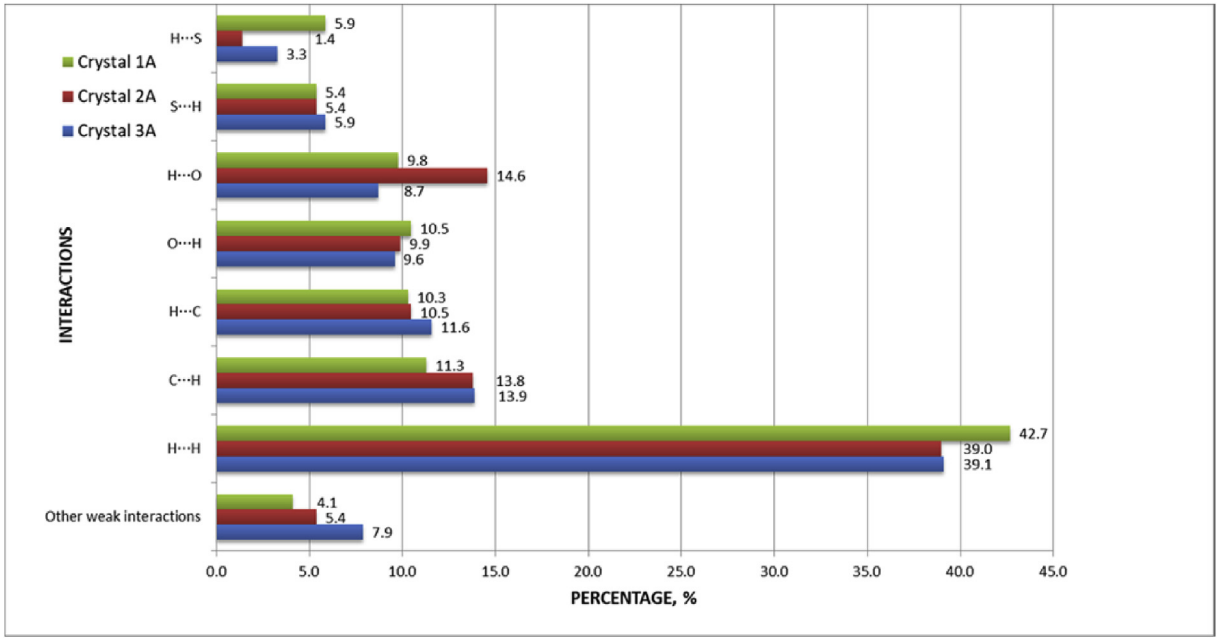

Fig. 11. Percentages of contact interactions contributions to the Hirshfeld surface areas in compounds **1A**, **2A** and **3A**.

Table 4
Inhibition percentage (I%) of the mycelial growth of *B. cinerea*, *R. solani* and *S. sclerotiorum* (after 3 days of incubation at 20 °C), *A. solani* (after 4 days of incubation at 25 °C), *C. acutatum* and *F. oxysporum* (after seven days of incubation at 25 °C) in the presence of the allyldithiocarbimate salt **1C** at 160 μM.

Fungi	I%	Fungi	I%
B. cinerea	70	*R. solani*	26
A. solani	31	*F. oxysporum*	12
S. sclerotiorum	30	*C. acutatum*	9

Table 5
Inhibition percentages of the mycelial growth of *B. cinerea* after 72 h of incubation at 20 °C in different concentrations of compounds **1A-E**, **2A-E** and **3A-E**.

Compound	Concentration/μM					
	5	10	20	40	120	160
	Inhibition (%)					
1A	1 ^{f}	20 ^{cd}	51 ^{a}	55 ^{ef}	65 ^{gh}	73 ^{cdef}
1B	1 ^{f}	12 ^{g}	41 ^{ef}	59 ^{c}	63 ^{h}	65 ^{j}
1C	1 ^{ef}	20 ^{cde}	46 ^{cd}	62 ^{b}	64 ^{gh}	70 ^{fgh}
1D	6 ^{c}	19 ^{def}	46 ^{cd}	59 ^{c}	65 ^{gh}	69 ^{hi}
1E	1 ^{def}	7 ^{h}	29 ^{h}	52 ^{h}	65 ^{gh}	70 ^{gh}
2A	20 ^{a}	22 ^{bc}	45 ^{d}	60 ^{c}	68 ^{cde}	75 ^{bc}
2B	6 ^{cd}	26 ^{a}	51 ^{a}	65 ^{a}	76 ^{a}	78 ^{a}
2C	4 ^{cdef}	23 ^{b}	45 ^{cd}	61 ^{b}	74 ^{b}	77 ^{a}
2D	4 ^{cdef}	27 ^{a}	48 ^{b}	61 ^{b}	67 ^{def}	71 ^{efgh}
2E	3 ^{cdef}	14 ^{g}	40 ^{f}	57 ^{d}	65 ^{fgh}	67 ^{ij}
3A	7 ^{c}	28 ^{a}	47 ^{bc}	57 ^{de}	67 ^{def}	73 ^{cde}
3B	11 ^{b}	23 ^{b}	40 ^{f}	56 ^{de}	66 ^{efg}	66 ^{j}
3C	5 ^{cde}	17 ^{f}	41 ^{f}	57 ^{de}	70^{c}	74^{cd}
3D	1 ^{f}	18 ^{ef}	43 ^{e}	54 ^{fg}	69^{cd}	72^{defg}
3E	2 ^{ef}	14 ^{g}	37 ^{g}	54 ^{g}	72^{b}	77^{ab}

$^{a-g}$Values presenting the same superscript letter, in the same column, do not differ at 5% level of significance by the Tukey test.

diseases [36–38]. The early blight disease due to *A. solani* causes significant loss in the potato production worldwide [39]. *R. solani* and *F. oxysporum* are soil-borne fungi. These plant pathogens are among the most difficult to control. *R. solani* causes pathogenic conditions such as black scurf in potato, leaf spot and root rot in tobacco, out of other plant diseases [40,41]. *F. oxysporum* affects various cultures and is the major limiting factor for tomato production, even in hydroponic cultivation systems [42,43]. *S. sclerotiorum* is a necrotrophic pathogen, which can also survive in the soil and affect hundreds of cultures. This broad host range makes it difficult to minimize the damages caused by *S. sclerotiorum* through crop rotation [44]. It is specially damaging to the soybean production, as no fungicide is able to offer complete control of the white mold disease [45–47].

We have previously demonstrated that the presence of a chlorine atom on the allyldithiocarbimate structure can enhanced its biological activity [6]. The salt shown in Fig. 1 was very active against *B. cinerea*, with an IC_{50} of 94 μM [6]. Thus the new allyldithiocarbimate **1C**, bearing a chlorine atom and a nitro group was chosen for the screening tests against the six fungi species. The results are shown in Table 4.

It can be inferred from Table 4 that the allyldithiocarbimate **1C** was active against the six species. It is also clear that the compound is selective, being more efficient in the control of *B. cinerea*, with 70% inhibition at 160 μM, while at the same dose, the mycelial growth inhibition of the other microorganisms were inferior to 31%.

Based on these results (Table 4), in order to deepen the biological studies on the allyldithiocarbimates, new *in vitro* tests against *B. cinerea* were performed with the whole series of analogues **1A-E**, **2A-E** and **3A-E**, at various concentrations, ranging from 5 to 160 μM. Table 5 shows the inhibition percentages calculated for each treatment. In addition, the Tukey test at 5% significance was applied to the data aiming the comparison of the results for each concentration tested.

From Table 5 it can be noted that the nitro group in *meta* position provided the best results, as in most cases the compounds **2A-E** were more active than their analogues **1A-E** or **3A-E**, with the same R groups. The halogens also presented a discrete contribution for the observed differences. The less active compound seems to be the allyldithiocarbimate **1E**, with a *para*-nitro group and an iodine atom, although it gets more effective at higher concentrations than a few other analogues. Compound **2B** present the best general performance, with the highest inhibition effect in almost all tested concentrations. This compound bears a *meta*-nitro group and a fluorine atom in the dithiocarbimate moiety. The fluorine atom does not cause great steric effects, as fluorine is a relatively small atom (resembling the hydrogen). However, it can change other properties related to electronic effects, interfering in intermolecular interactions and in the physical properties of the substance. Thus, the number of fungicides bearing fluorine atoms is expressive, especially aromatic-fluorine compounds [48,49]. Fig. 12 shows a comparison of the activity of **2B** and the less active allyldithiocarbimate **1E,** at 20 μM.

Using the whole set of data collected for *B. cinerea* it was possible to plot dose-response curves, as exemplified in Fig. 13. From the dose-response equations it was possible to calculate the IC_{50} values for each substance (Table 6). Although compounds **1A**, **2B** and **2D** presented similar IC_{50} values (Table 6), an inspection on Table 5 shows that **2B** was more active than these compounds in almost all concentrations tested. The results indicate that compound **2B** is a target compound for the development of a new fungicide to control *Botrytis* diseases.

The presence of a nitro group can change the activity of a

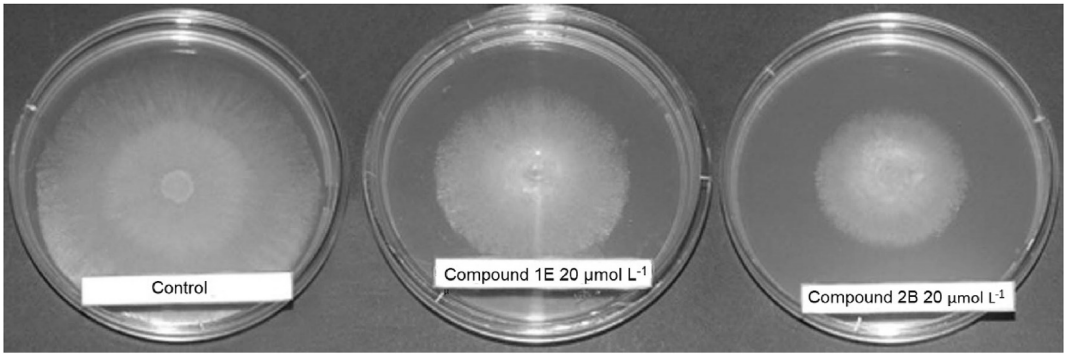

Fig. 12. Photograph showing the mycelial growth of *B. cinerea* in the presence of the allyldithiocarbimates **1E** and **2B** at 20 μM compared to the control.

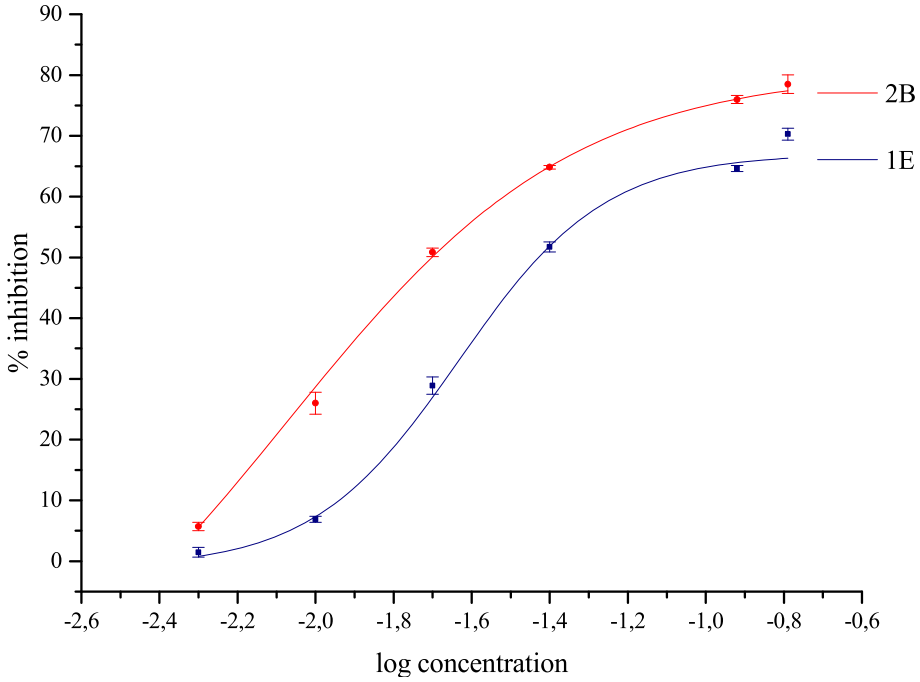

Fig. 13. Inhibition percentages of the mycelial growth of *B. cinerea*: comparison of dose-response curves for the less (**1E**) and the most (**2B**) active allyldithiocarbimates.

Table 6
Concentration of compounds **1A-E**, **2A-E** and **3A-E** for the inhibition of 50% of the mycelial growth of *B. cinerea* (IC_{50}), over the control.

Compound	IC_{50} (μM)	Compound	IC_{50} (μM)	Compound	IC_{50} (μM)
1A	20	**2A**	24	**3A**	26
1B	25	**2B**	20	**3B**	29
1C	23	**2C**	23	**3C**	29
1D	24	**2D**	21	**3D**	29
1E	37	**2E**	28	**3E**	33

Table 7
Concentration of compounds **4A-E** and **5A-E** for the inhibition of 50% of the mycelial growth of *B. cinerea* (IC_{50}), over the control [6].

Compound	IC_{50} (μM)	Compound	IC_{50} (μM)
4A	100	**5A**	47
4B	130	**5B**	41
4C	94	**5C**	38
4D	95	**5D**	46
4E	130	**5E**	49

molecule, interacting with enzymes, cell membranes and target receptors, or producing secondary activity reactions [50,51]. In fact, the introduction of the nitro group in the structure of the allyldithiocarbimates was the most important feature for the activity against *B. cinerea*. While the allyldithiocarbimates **1A-E**, **2A-E** and **3A-E** presented IC_{50} between 20 and 37 μM, their analogues without the nitro group (Fig. 14, compouds **4A-E**) showed IC_{50} values in the range of 94–130 μM (Table 7), using the same testing methodology [6]. The new compounds were also more active than other analogues derived from furfuraldehyde (Fig. 14, compouds **5A-E**) with IC_{50} of 38–56 μM (Table 7) [6].

The influence of the parent allylic bromides (Scheme 1) on the mycelial growth of *B. cinerea* was tested at 160 μM, for comparison purposes. The potassium dithiocarbimates were not included in the tests as they are not very stable in solution, showing high degree of decomposition after 24 hours in aqueous media. The inhibition percentages of the treatments with the allylic bromides were of only 14% (*para*-nitro group), 25% (*meta*-nitro group) and 22% (*ortho*-nitro group), while at the same concentration, the allyldithiocarbimate salts had inhibition ranges of 65–78%. It is interesting to note that the allylic bromide with the nitro group in *meta* position was more active than the *para* and *ortho* analogues, as it was observed with the series **1A-E**, **2A-E** and **3A-E**.

Two metal-dithiocarbamates used as commercial fungicides, Ziram and Mancozeb, were also tested against *B. cinerea* in the same conditions, at 160 μM. The new allyldithiocarbimates were also more active than these fungicides, which inhibited the growth of *B. cinerea* by 16% (Ziram) and 8% (Mancozeb). Thus, the new allyldithiocarbimate salts are more active than dithiocarbamates widely used as agrochemicals.

4. Conclusion

In this work, the steps required for the synthesis of 15 new tetraphenylphosphonium allyldithiocarbimates derived from Morita-Baylis-Hillman adducts bearing nitro groups have been described. The new substances were synthesized in good yields (63–97%) and had their structures confirmed by IR and NMR spectroscopy, high-resolution mass spectrometry as well as single crystal X-ray diffraction. The X-ray diffraction evidenced the *Z* stereochemistry of the allyldithiocarbimate anions. The X-ray data for the compounds **1A**, **2A** and **3A** revealed that the crystal packing are mainly stabilized by the electrostatic interactions between oppositely charged ions as well as C–H···O intramolecular and intermolecular interactions. Molecular electrostatic potentials mapped for these compounds were correlated with the decrease of melting points depending on the position of the nitro group on the aromatic ring: *para* > *meta* > *ortho*. This explains the ionic liquid

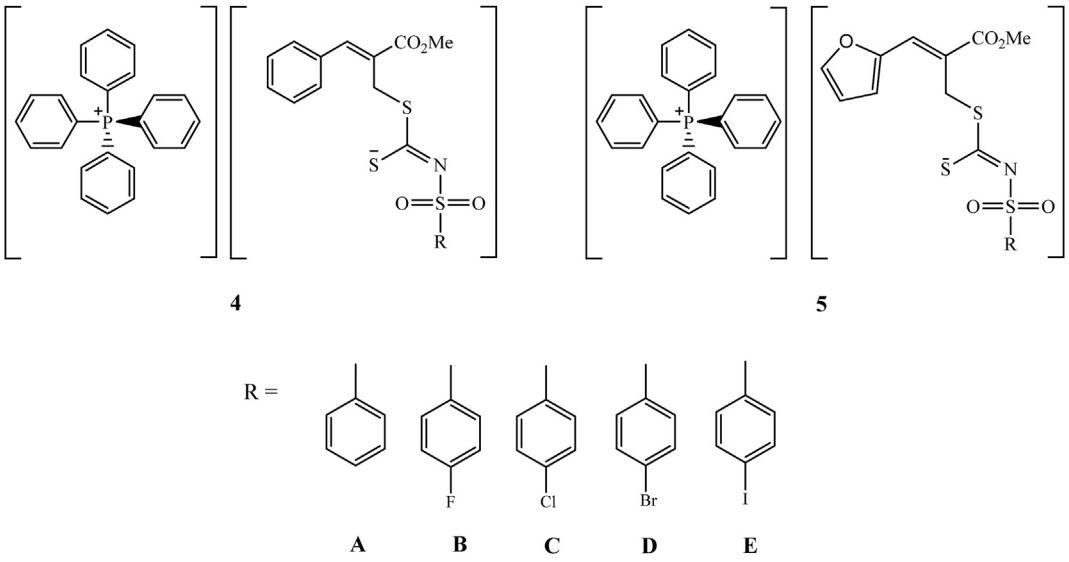

Fig. 14. Published allyldithiocarbimates [6].

behavior of the salts of the series **3A-E**. The 2D fingerprint plots for the compounds **1A**, **2A** and **3A**, together with the contribution percentages of different interactions to their Hirshfield surfaces, provided a more complete understanding of the intermolecular interactions present in the crystal.

The allyldithiocarbimates strongly inhibit the mycelial growth of *B. cinerea*, with little effect on other fungi species. The new compounds are more effective against *B. cinerea* than the active principals of the commercial fungicides Ziram and Mancozeb. The presence of a nitro group on the allyldithiocarbimate structure increases its activity towards *B. cinerea*, especially when the nitro group is in *meta* position, with IC_{50} values between 20 and 28 μM, depending on the presence of the various halogen substituents tested.

The compound **2B**, presenting a *meta*-nitro group and a *para*-fluorine atom (in different aromatic rings) presented the best overall performance. With an IC_{50} of only 20 μM, **2B** is a target substance for the development of a new agrochemical for the control plant diseases caused by *Botrytis*.

Declaration of competing interest

The authors declare that they have no known competing financial interests or personal relationships that could have appeared to influence the work reported in this paper.

Acknowledgements

We are grateful to the Fundação de Amparo à Pesquisa do Estado de Minas Gerais (FAPEMIG, Brazil, Grant APQ-02382-17), Conselho Nacional de Desenvolvimento Científico e Tecnológico (CNPq, Brazil, J.E. grant #305190/2017-2), Fundação de Amparo à Pesquisa do Estado de São Paulo (FAPESP, Brazil Grants 2016/08823-4 and 2013/07581-3) and Coordenação de Aperfeiçoamento de Pessoal de Nivel Superior (CAPES, Brazil) for financial support and research fellowships. We thank the Núcleo de Análise de Biomoléculas of the Universidade Federal de Viçosa for providing the facilities for HRMS experiments. We are grateful to Prof. Dr. Christian Lehmann and all the staff of the Chemical Crystallography Department from Max-Planck Institute for Coal Research (Mülheim a.d. Ruhr – Germany) for the use of the X-ray diffractometer equipment. We thank the Laboratório de Celulose e Papel of the Universidade Federal de Viçosa for the elemental analysis of C, H and N.

Supplementary material

Details on data collection, refinement and crystallographic data in CIF format for structures **1A**, **2A** and **3A** have been deposited at the Cambridge Crystallographic Data Centre, CCDC 1966804 (compound **1A**), CCDC 1966805 (compound **2A**) and CCDC 1966806 (compound **3A**). Copies of this information may be obtained free of charge from The Director, CCDC, 12 Union Road, Cambridge, CB21EZ, UK (fax: +44 1223 336 033; email: deposit@ccdc.cam.ac.uk or http://www.ccdc.cam.ac.uk).

References

[1] P.E. Russell, Centenary Review: a century of fungicide evolution, J. Agric. Sci. 143 (2005) 11–25, https://doi.org/10.1017/S0021859605004971.
[2] M.L. Gullino, F. Tinivella, A. Garibaldi, G.M. Kemmitt, L. Bacci, B. Sheppard, Mancozeb: past, present and future, Plant Dis. 94 (2010) 1076–1087, https://doi.org/10.1094/PDIS-94-9-1076.
[3] M. Hahn, The rising threat of fungicide resistance in plant pathogenic fungi: *Botrytis* as a case study, J. Chem. Biol. 7 (2014) 133–141, https://doi.org/10.1007/s12154-014-0113-1.
[4] K.W. Weissmahr, D.L. Sedlak, Effect of metal complexation on the degradation of dithiocarbamate fungicides, Environ. Toxicol. Chem. 19 (2000) 820–826, https://doi.org/10.1002/etc.5620190406.
[5] P.J. Nieuwenhuizen, A.W. Ehlers, J.G. Haasnoot, S.R. Janse, J. Reedijk, E.-J. Baerends, Mechanism of zinc(II) dithiocarbamate accelerated vulcanization uncovered: theoretical and experimental evidence, J. Am. Chem. Soc. 121 (1999) 163–168, https://doi.org/10.1021/ja982217n.
[6] E.C. Tavares, M.M.M. Rubinger, E.V. Filho, M.R.L. Oliveira, D. Piló-Veloso, J. Ellena, S. Guilardi, R.A.C. Souza, L. Zambolim, Tetraphenylphosphonium allyldithiocarbimates derived from Morita-Baylis-Hillman adducts: synthesis, characterization, crystal structure and antifungal activity, J. Mol. Struct. 1106 (2016) 130–140, https://doi.org/10.1016/j.molstruc.2015.10.097.
[7] R. Dean, J.A.L. Van Kan, Z.A. Pretorius, K.E. Hammond-Kosack, A. Di Pietro, P.D. Spanu, J.J. Rudd, M. Dickman, R. Kahmann, J. Ellis, G.D. Foster, The top 10 fungal pathogens in molecular plant pathology, Mol. Plant Pathol. 13 (2012) 414–430, https://doi.org/10.1111/j.1364-3703.2011.00783.x.
[8] B.T. Gowda, K. Jyothi, J.D. D'souza, Infrared and NMR spectra of arylsulphonamides, 4-X-$C_6H_4SO_2NH_2$ and i-X, j-$YC_6H_4SO_2NH_2$ (X=CH_3; C_2H_5; F; Cl; Br; I; or NO_2 and i-X, j-Y=2,3-$(CH_3)_2$; 2,4-$(CH_3)_2$; 2,5-$(CH_3)_2$; 2-CH_3, 4-Cl; 2-CH_3, 5-Cl; 3-CH_3, 4-Cl; 2,4-Cl_2 or 3,4-Cl_2, Z. Naturforsch. A 57 (2002) 967–973, https://doi.org/10.1515/zna-2002-1210.
[9] K. Hartke, Darstellung von sulfonylisothiocyanaten, Arch. Pharm. 299 (1966) 174–178, https://doi.org/10.1002/ardp.19662990212.
[10] R.S. Amim, M.R.L. Oliveira, G.J. Perpétuo, J. Janczak, L.D.L. Miranda, M.M.M. Rubinger, Syntheses, crystal structure and spectroscopic

characterization of new platinum(II) dithiocarbimato complexes, Polyhedron 27 (2008) 1891–1897, https://doi.org/10.1016/j.poly.2008.02.030.
[11] H.U. Hummel, U. Korn, Dithiocarbimates from sulfonamides, Part 1: preparation and X-ray crystal structures of $K_2[S_2C{=}N\text{-}SO_2\text{-}C_6H_5].2H_20$ and $K_2[S_2C{=}N\text{-}SO_2\text{-}C_6H_4\text{-}Cl].2H_20$, Z, Naturforsch B 44 (1989) 24–28, https://doi.org/10.1515/znb-1989-0109.
[12] M.R.L. Oliveira, V.M. De Bellis, Preparation of novel cobalt(III) complexes with dithiocarbimates derived from sulfonamides, Transit. Met. Chem. 24 (1999) 127–130, https://doi.org/10.1023/A:1006945923839.
[13] M.R.L. Oliveira, M.M.M. Rubinger, V.M. De Bellis, Preparation of novel palladium(II) complexes with dithiocarbimates from sulfonamides, Transit. Met. Chem. 28 (2003) 455–459, https://doi.org/10.1023/A:1023676403383.
[14] E.F. Franca, M.R.L. Oliveira, S. Guilardi, R.P. Andrade, R.H. Lindemann, J. Amim Jr., J. Ellena, V.M. De Bellis, M.M.M. Rubinger, Preparation, crystal structure and spectroscopic characterization of nickel(II) complexes with dithiocarbimate derivated of sulfonamides, Polyhedron 25 (2006) 2119–2126, https://doi.org/10.1016/j.poly.2005.11.035.
[15] C.G. Lima-Junior, P.A.C. Assis, F.P.L. Silva, S.C.O. Sousa, N.G. de Andrade, T.P. Barbosa, P.L.N. Nerís, L.V.G. Segundo, I.C. Anjos, G.A.U. Carvalho, G.B. Rocha, M.R. Oliveira, M.L.A.A. Vasconcellos, Efficient synthesis of 16 aromatic Morita-Baylis-Hillman adducts: biological evaluation on *Leishmania amazonensis and Leishmania chagasi*, Bioorg. Chem. 38 (2010) 279–284, https://doi.org/10.1016/j.bioorg.2010.08.002.
[16] M. Ferreira, L. Fernandes, M.M. Sá, A highly efficient and general method for the preparation of (*Z*)-allylic bromides derived from Morita-Baylis-Hillman adducts, J. Braz. Chem. Soc. 20 (2009) 564–568, https://doi.org/10.1590/S0103-50532009000300023.
[17] J.S. Yadav, B.V.S. Reddy, C. Madan, Montmorillonite clay-catalyzed stereoselective syntheses of aryl-substituted (*E*)- and (*Z*)-allyl iodides and bromides, New J. Chem. 25 (2001) 1114–1117, https://doi.org/10.1039/B103850H.
[18] M.M. Sá, M. Ferreira, E.S. Lima, I. Santos, P.P. Orlandi, L. Fernandes, Antimicrobial activity of allylic thiocyanates derived from the Morita-Baylis-Hillman reaction, Braz. J. Microbiol. 45 (2014) 807–812, https://doi.org/10.1590/S1517-83822014000300007.
[19] APEX2 Version 2.1-0, Bruker AXS Inc. Madison, 2004.
[20] SAINT Version 7.46a, Bruker AXS Inc. Madison, 2004.
[21] G.M. Sheldrick, TWINABS, Version 2012/1, Georg-August-Universität Göttingen, Göttingen, Germany, 2012.
[22] O.V. Dolomanov, L.J. Bourhis, R.J. Gildea, J.A.K. Howard, H. Puschmann, OLEX2: a complete structure solution, refinement and analysis program, J. Appl. Crystallogr. 42 (2009) 339–341, https://doi.org/10.1107/S0021889808042726.
[23] L.J. Bourhis, O.V. Dolomanov, R.J. Gildea, J.A.K. Howard, H. Puschmann, The anatomy of a comprehensive constrained, restrained refinement program for the modern computing environment - Olex2 dissected, Acta Crystallogr. A71 (2015) 59–75, https://doi.org/10.1107/S2053273314022207.
[24] G.M. Sheldrick, Crystal structure refinement with SHELXL, Acta Crystallogr. C71 (2015b) 3–8, https://doi.org/10.1107/S2053229614024218.
[25] G.M. Sheldrick, SADABS, University of Göttingen, Göttingen, 1996.
[26] L. Farrugia, WinGX and ORTEP for windows: an update, J. Appl. Crystallogr. 45 (2012) 849–854.
[27] C.F. Macrae, P.R. Edgington, P. McCabe, E. Pidcock, G.P. Shields, R. Taylor, M. Towler, J. van de Streek, Mercury: visualization and analysis of crystal structures, J. Appl. Crystallogr. 39 (2006) 453–457, https://doi.org/10.1107/S002188980600731X.
[28] S.K. Wolff, D.J. Grimwood, J.J. McKinnon, D. Jayatilaka, M.A. Spackman, Crystal Explorer 2.1, University of Western Australia, Perth, 2007.
[29] L.C. Alves, M.M.M. Rubinger, R.H. Lindemann, G.J. Perpétuo, J. Janczak, L.D.L. Miranda, L. Zambolim, M.R.L. Oliveira, Syntheses, crystal structure, spectroscopic characterization and antifungal activity of new N-*R*-Sulfonyldithiocarbimate metal complexes, J. Inorg. Biochem. 103 (2009) 1045–1053, https://doi.org/10.1016/j.jinorgbio.2009.04.018.
[30] L.C. Alves, M.M.M. Rubinger, E.C. Tavares, J. Janczak, E.B.A.V. Pacheco, L.L.Y. Visconte, M.R.L. Oliveira, Syntheses, spectroscopic characterization, crystal structure and natural rubber vulcanization activity of new disulfides derived from sulfonyldithiocarbimates, J. Mol. Struct. 1048 (2013) 244–251, https://doi.org/10.1016/j.molstruc.2013.05.062.
[31] J. Li, Cyclohexanaminium 3,4,5,6-tetrachloro-2-(methoxycarbonyl)benzoate, Acta Crystallogr. E67 (2011) o842, https://doi.org/10.1107/S1600536811008531.
[32] C.E. Wagner, T.L. Groy, 2-Fluoro-4-(methoxycarbonyl)benzoic acid, Acta Crystallogr. E66 (2010) o2340, https://doi.org/10.1107/S1600536810032253.
[33] F.H. Allen, O. Kennard, D.G. Watson, L. Brammer, A.G. Orpen, R. Taylor, Tables of bond lengths determined by X-ray and neutron diffraction. Part 1. Bond lengths in organic compounds, J. Chem. Soc. Perkin Trans. 2 (1987) S1–S19, https://doi.org/10.1039/p298700000s1.
[34] M.C. Etter, Encoding and decoding hydrogen-bond patterns of organic compounds, Acc. Chem. Res. 23 (1990) 120–126, https://doi.org/10.1021/ar00172a005.
[35] G. Romanazzi, J.L. Smilanick, E. Feliziani, S. Drobyc, Integrated management of postharvest gray mold on fruit crops, Postharvest Biol. Technol. 113 (2016) 69–76, https://doi.org/10.1016/j.postharvbio.2015.11.003.
[36] J. Moral, R. Oliveira, A. Trapero, Elucidation of the disease cycle of olive anthracnose caused by *Colletotrichum acutatum*, Phytopathology 99 (2009) 548–556, https://doi.org/10.1094/PHYTO-99-5-0548.
[37] B.S.G. Paredes, F.R. Muñoz, Effect of different fungicides in the control of *Colletotrichum acutatum*, causal agent of anthracnose crown rot in strawberry plants, Crop Protect. 21 (2002) 11–15, https://doi.org/10.1016/S0261-2194(01)00054-0.
[38] S. Freeman, Y. Nizani, S. Dotan, S. Even, T. Sando, Control of *Colletotrichum acutatum* in strawberry under laboratory, greenhouse, and field conditions, Plant Dis. 81 (1997) 749–752, https://doi.org/10.1094/PDIS.1997.81.7.749.
[39] I.K. Abuley, B.J. Nielsen, Evaluation of models to control potato early blight (*Alternaria solani*) in Denmark, Crop Prot. 102 (2017) 118–128, https://doi.org/10.1016/j.cropro.2017.08.012.
[40] D. Atkinson, M.K. Thornton, J.S. Miller, Development of *Rhizoctonia solani* on stems, stolons and tubers of potato II. Efficacy of chemical applications, Am. J. Pot. Res. 88 (2011) 96–103, https://doi.org/10.1007/s12230-010-9172-1.
[41] M. Gonzalez, M. Pujol, J.P. Metraux, V. Gonzalez-Garcia, M.D. Bolton, O. Borrás-Hidalgo, Tobacco leaf spot and root rot caused by *Rhizoctonia solani Kühn*, Mol. Plant Pathol. 12 (2011) 209–216, https://doi.org/10.1111/j.1364-3703.2010.00664.x.
[42] R. Joshi, A review of *Fusarium oxysporum* on its plant interaction and industrial use, J. Med. Plants. Stud. 6 (2018) 112–115, https://doi.org/10.22271/plants.2018.v6.i3b.07.
[43] R.J. Mcgovern, Management of tomato diseases caused by *Fusarium oxysporum*, Crop Protect. 73 (2015) 78–92, https://doi.org/10.1016/j.cropro.2015.02.021.
[44] G.J. Boland, R. Hall, Index of plant hosts of *Sclerotinia sclerotiorum*, Can. J. Plant Pathol. 16 (1994) 93–108, https://doi.org/10.1080/07060669409500766.
[45] A.J. Peltier, C.A. Bradley, M.I. Chilvers, D.K. Malvick, D.S. Mueller, K.A. Wise, P.D. Esker, Biology, yield loss and control of *sclerotinia* stem rot of soybean, J. Integr. Pest Manag. 3 (2012) B1–B7, https://doi.org/10.1603/IPM11033.
[46] M. Mccaghey, J. Willbur, D.L. Smith, M. Kabbage, The complexity of the *Sclerotinia sclerotiorum* pathosystem in soybean: virulence factors, resistance mechanisms, and their exploitation to control *Sclerotinia* stem rot, Trop. Plant Pathol. 44 (2019) 12–22, https://doi.org/10.1007/s40858-018-0259-4.
[47] U. Smolińska, B. Kowalska, Biological control of the soil-borne fungal pathogen *Sclerotinia sclerotiorum* - a review, J. Plant Pathol. 100 (2018) 1–12, https://doi.org/10.1007/s42161-018-0023-0.
[48] G. Theodoridis, Fluorine-containing agrochemicals: an overview of recent developments, Adv. Fluorine Sci. 2 (2006) 121–175, https://doi.org/10.1016/S1872-0358(06)02004-5.
[49] P. Jeschke, Latest generation of halogen-containing pesticides, Pest Manag. Sci. 73 (2017) 1053–1066, https://doi.org/10.1002/ps.4540.
[50] D. Olender, J. Zwawiak, L. Zaprutko, Multidirectional efficacy of biologically active nitro compounds included in medicines, Pharmaceuticals 11 (2018) 54–83, https://doi.org/10.3390/ph11020054.
[51] C.G. Lima–Junior, M.L.A.A. Vasconcellos, Morita–Baylis–Hillman adducts: biological activities and potentialities to the discovery of new cheaper drugs, Bioorg. Med. Chem. 20 (2012) 3954–3971, https://doi.org/10.1016/j.bmc.2012.04.061.